Cell

Intercellular Nanotubes Mediate Bacterial Communication

Gyanendra P. Dubey[1] and Sigal Ben-Yehuda[1,*]
[1]Department of Microbiology and Molecular Genetics, Institute for Medical Research Israel-Canada (IMRIC), The Hebrew University-Hadassah Medical School, POB 12272, The Hebrew University of Jerusalem, 91120 Jerusalem, Israel
*Correspondence: sigalb@ekmd.huji.ac.il
DOI 10.1016/j.cell.2011.01.015

SUMMARY

Bacteria are known to communicate primarily via secreted extracellular factors. Here we identify a previously uncharacterized type of bacterial communication mediated by nanotubes that bridge neighboring cells. Using *Bacillus subtilis* as a model organism, we visualized transfer of cytoplasmic fluorescent molecules between adjacent cells. Additionally, by coculturing strains harboring different antibiotic resistance genes, we demonstrated that molecular exchange enables cells to transiently acquire nonhereditary resistance. Furthermore, nonconjugative plasmids could be transferred from one cell to another, thereby conferring hereditary features to recipient cells. Electron microscopy revealed the existence of variously sized tubular extensions bridging neighboring cells, serving as a route for exchange of intracellular molecules. These nanotubes also formed in an interspecies manner, between *B. subtilis* and *Staphylococcus aureus*, and even between *B. subtilis* and the evolutionary distant bacterium *Escherichia coli*. We propose that nanotubes represent a major form of bacterial communication in nature, providing a network for exchange of cellular molecules within and between species.

INTRODUCTION

Bacteria in nature display complex multicellular behaviors that enable them to execute sophisticated tasks such as antibiotic production, secretion of virulence factors, bioluminescence, sporulation, and competence for DNA uptake (Bassler and Losick, 2006; Lazazzera, 2001; Nealson et al., 1970; Ng and Bassler, 2009; Tomasz, 1965). Such social activities ultimately benefit the population and are unproductive if performed by a single bacterium. Furthermore, nearly all bacteria are capable of forming a resilient multicellular structure, termed biofilm, comprising cells with different functionalities. Natural biofilms are typically composed of several bacterial species and therefore demand a coordinated gene expression of the various inhabitants (Kolter and Greenberg, 2006; Kuchma and O'Toole, 2000; Lemon et al., 2008; Straight and Kolter, 2009).

Multicellular activity is achieved by the ability of group members to exchange information in order to synchronize their behavior. Importantly, bacteria are not limited to communicate within their own species but are also capable of sending and receiving messages in an interspecies manner. In both Gram-positive and -negative bacteria, cell-to-cell exchange of information is mediated primarily by signaling molecules belonging to the general classes of low molecular weight autoinducers and signaling oligopeptides (Bassler and Losick, 2006; Fuqua and Greenberg, 2002; Lazazzera, 2001; Ng and Bassler, 2009). In a process known as quorum sensing (QS), the production and detection of these signaling molecules is employed by bacteria to monitor population density and modulate gene expression accordingly (Bassler and Losick, 2006; Fuqua and Greenberg, 2002; Lazazzera, 2001; Nealson et al., 1970; Ng and Bassler, 2009; Tomasz, 1965).

Secretion and detection of small extracellular molecules to the surrounding environment is not the only form of molecular exchange between bacteria. Many Gram-negative bacteria trade information by packaging molecules into extracellular membrane vesicles (MVs). These MVs can travel and fuse with distal cells, thus providing a secure mode for delivering various cellular moieties, including QS molecules, antimicrobial factors, toxins, and DNA (Mashburn-Warren and Whiteley, 2006). Furthermore, in some cases neighboring daughter cells have been found to exchange molecular information by establishing intimate cytoplasmic connections. In cyanobacteria, for example, the movement of small molecules (e.g; sugars and amino acids) within a filament was shown to be mediated by intercellular channels. This cytoplasmic sharing enables vital cooperative behavior between nitrogen fixing heterocysts and photosynthetic nurturing cells (Giddings and Staehelin, 1981; Golden and Yoon, 2003; Mullineaux et al., 2008).

An additional type of molecular exchange that involves physical interactions between neighboring bacterial cells is conjugation (Lederberg and Tatum, 1946). During this process DNA is transferred from a donor to a recipient through a pilus, a tube-like structure that physically connects the participating cells (Madigan et al., 2003). Notably, conjugation represents a key mechanism of horizontal gene transfer in nature (Juhas et al., 2009), whereby hereditary genetic information, rather than nonhereditary molecular signal, is delivered.

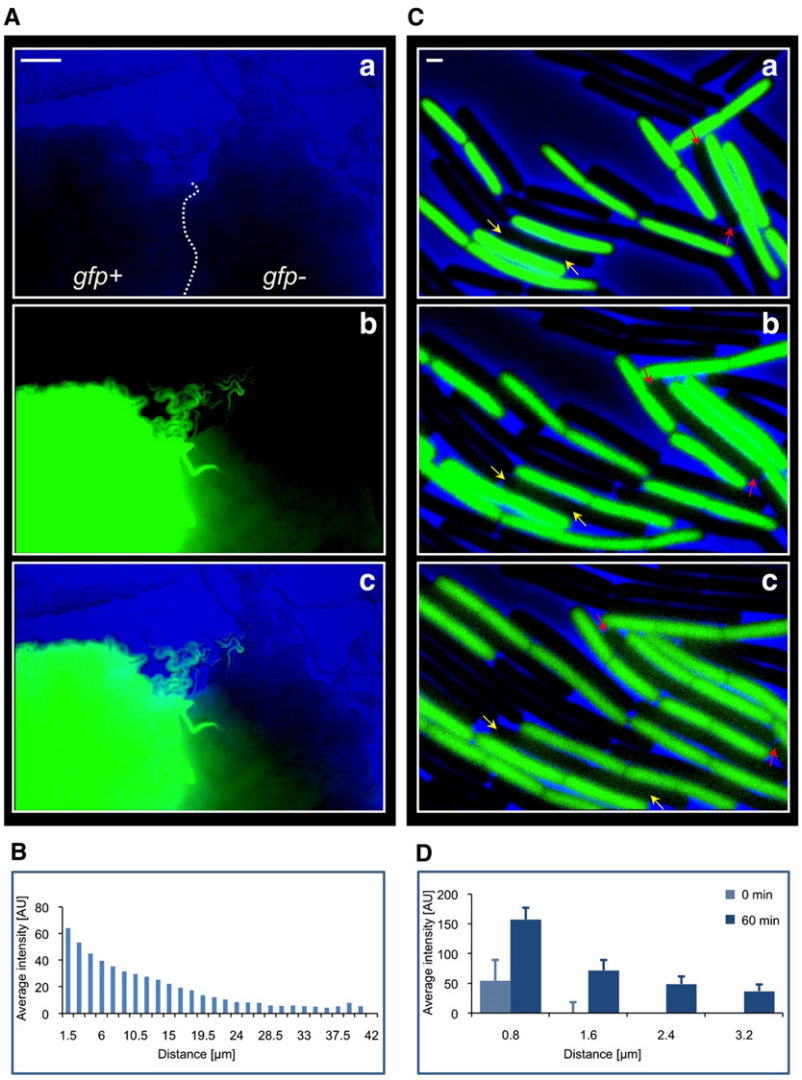

Figure 1. Visualizing a Molecular Gradient between Neighboring *B. subtilis* Cells

(A) PY79 (*gfp*−) and SB444 (*gfp*+) cells were grown side by side on an LB agar plate at 37°C and visualized by fluorescence microscopy 15 hr after plating, when small colonies were visible. The dashed line indicates the border between the two populations. (a) Phase contrast image (blue). (b) GFP fluorescence image (green). (c) Overlay of phase and GFP fluorescence images. The scale bar represents 10 μm.

(B) Average fluorescence intensity of the *gfp*− population (as indicated in Aa) as a function of the distance from the *gfp*+ population. The *gfp*− region was divided into identical sub-regions and the average fluorescence signal was defined in arbitrary units (AU).

(C) Exponentially growing PY79 (*gfp*−) and SB444 (*gfp*+) cells were mixed, plated on an LB agarose pad, and incubated in a temperature controlled chamber at 37°C. Cells were visualized by time-lapse fluorescence microscopy and phase contrast (blue) and fluorescence (green) images collected at 10 min intervals. Select overlay images are shown from the following time points: (a) t0 min, (b) t30 min, and (c) t60 min. Each pair of colored arrows (red and yellow) indicates different locations where transfer of fluorescent molecules between neighboring cells is increasing over time. Larger fields of the same region are shown in Figure S1. The scale bar represents 1 μm.

(D) Average fluorescence intensity of the *gfp*− cells as a function of their distance from the *gfp*+ cells at t0 min (light blue bars) and at t60 min (dark blue bars) of the co-incubation experiment as described in (C) (see Extended Experimental Procedures). No detectible signal was measured when cells were located beyond 1 μm at t0 min. Average fluorescence signal is expressed in arbitrary units (AU). Error bars represent standard deviation (SD) of the mean fluorescence signal calculated from at least 40 cells located at the indicated distance. Shown is a representative experiment out of three independent biological repeats.

See also Figure S1 and Figure S2.

Tubular conduits between cells that allow exchange of cellular content are typical of multicellular organisms. In plants, neighboring cells are connected by cytoplasmic tubes called plasmodesmata, which provide multiple routes for intercellular transfer of nutrients, signals, proteins and transcripts (Heinlein and Epel, 2004; Lucas et al., 2009). In mammalian cells, intercellular communication is mediated locally through gap junctions and synapses; however, recent reports demonstrate the existence of a network of intercellular membrane nanotubes enabling long-distance communication. These tunneling nanotubes have been shown to facilitate intercellular transfer of cytoplasmic molecules and even organelles and viruses (Belting and Wittrup, 2008; Hurtig et al., 2010; Schara et al., 2009). Here we report the identification of analogous nanotubular channels formed among bacterial cells grown on solid surface. We demonstrate that nanotubes connect bacteria of the same and different species, thereby providing an effective conduit for exchange of intracellular content.

RESULTS

Neighboring *B. subtilis* Cells Exchange Cytoplasmic Constituents

Given the complex intercellular communication required within natural bacterial communities, we reasoned that bacterial cells grown on a solid surface can physically interact in order to establish an effective route for exchange of molecular information. Initially, we examined whether adjacent cells exchange cytoplasmic GFP molecules. *Bacillus subtilis* cells (SB444) harboring a chromosomally encoded *gfp* reporter gene (*gfp*+) were spotted on solid medium alongside *B. subtilis* cells (PY79) lacking *gfp* (*gfp*−). Cells were allowed to grow for 15 hr and then visualized by fluorescence microscopy (Figure 1A). Remarkably, a green fluorescence gradient was observed to emanate from the *gfp*+ cells toward the *gfp*− cells, covering a distance of approximately 40 μm (Figures 1Ab and 1B). Superimposing the green fluorescence and the phase contrast image, which demarcates the cells

boundary, demonstrated that this fluorescence gradient was associated exclusively with the presence of cells (Figure 1Ac). The observed cell-associated gradient of the GFP signal concords with our premise that cytoplasmic molecular exchange occurs between neighboring cells. However, it remained possible that the gradient was due to migrating *gfp*+ cells.

To further explore this phenomenon, time-lapse microscopy was carried out to follow the formation of the GFP gradient at a single-cell level. *gfp*+ and *gfp*− cells were mixed, applied to an agarose pad, and their growth and fluorescence were monitored. Immediately after mixing (t0 min), the fluorescence signal was confined to the *gfp*+ cells and no detectable fluorescence was seen in adjacent *gfp*− cells (Figure 1Ca). However, after 30 min, *gfp*− cells lying in proximity to *gfp*+ cells acquired a weak fluorescence signal (Figure 1Cb). The fluorescence intensity of *gfp*− cells increased over time in a manner inversely proportional to their distance from the *gfp*+ cells, i.e.: cells residing closer to the *gfp*+ cells acquired more fluorescence than distant ones (Figure 1D). Conversely, the fluorescence displayed by *gfp*+ cells decreased over time (Figure 1Cc), suggesting that they distribute their fluorescence among proximal cells. Observing a larger field highlights that as time progresses, *gfp*− cells not directly contacting *gfp*+ cells, also gained a fluorescence signal (Figure S1A available online). To rule out the possibility that these observations are a consequence of multiple fluorescence exposures, we imaged unexposed regions of the growing cells at the final time point, and a similar fluorescence pattern was detected (Figure S1B). Further, when *gfp*+ and *gfp*− cells were residing apart from one other, neither the *gfp*− cells gained nor the *gfp*+ cells lost fluorescence (Figure S2). The contact-dependent nature of the fluorescence gradient excludes the possibility that the signal derives from cell migration and corroborates that cytoplasmic GFP molecules (27 kDa) can be transferred from one cell to another in a temporal and spatial manner. Of note, we cannot exclude the possibility that to some extent *gfp* transcripts are also being traded among the cells.

In a complementary approach, cytoplasmic exchange was examined with calcein, a nongenetically encoded cytoplasmic fluorophore. Calcein is a small nonfluorescent acetoxymethylester (AM) derivative that is sufficiently hydrophobic to traverse cell membranes. After passage into the cytoplasm, hydrolysis of calcein by endogenous esterases gives rise to a fluorescent hydrophilic product (623 Da) unable to traverse membranes and thus caged within the cytoplasm (Haugland, 2005). When *B. subtilis* cells (PY79) were incubated with calcein-AM (see Extended Experimental Procedures), they rapidly acquired a strong fluorescence signal indicating calcein hydrolysis. Next, labeled cells were washed, mixed with nonlabeled cells, and the mixture was placed on an agarose pad and tracked by time-lapse microscopy. At t0 min, only labeled cells exhibited a detectable fluorescence signal (Figures 2A and 2A′). After 15 min, an apparent fluorescence signal was monitored from nonlabeled cells located in the vicinity of labeled ones (Figures 2B and 2B′). Remarkably, however, by t30 min almost all the nonlabeled cells displayed significant fluorescence while the fluorescence from labeled cells decreased (Figures 2C and 2C′ and Figure S3Ba). When unexposed regions of the growing cells were photographed at the latest time point, a similar fluorescence pattern

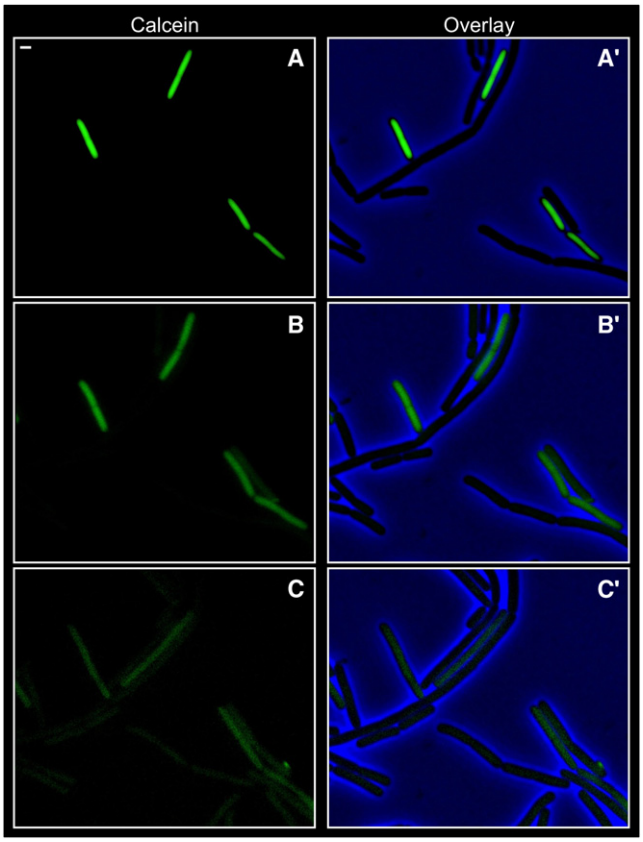

Figure 2. Transfer of Calcein between Neighboring *B. subtilis* Cells
Exponentially growing PY79 cells were labeled with calcein (see Extended Experimental Procedures). Labeled cells were washed and mixed with nonlabeled cells, plated on an LB agarose pad, and incubated in a temperature controlled chamber at 37°C. Cells were visualized by time-lapse fluorescence microscopy and images of phase contrast (blue) and fluorescence (green) were collected at 5 min intervals. Select fluorescence (A–C) and corresponding overlay images (A′–C′) are shown from the following time points: (A and A′) t0 min, (B and B′) t15 min, and (C and C′) t30 min. The scale bar represents 1 μm. See also Figure S3.

was observed (data not shown). Consistently, labeled cells, located apart from nonlabeled ones, largely maintained their fluorescence signal (Figure S3A). Thus, same as GFP, calcein can be transferred from one cell to another; yet it appears to be delivered more rapidly, suggesting that the speed of transfer inversely correlates with the size of the traversed molecule.

Taken together, our results establish that adjacent *B. subtilis* cells are able to exchange cytoplasmic molecules in a spatially ordered manner. To the best of our knowledge, this is the first report of cytoplasmic sharing between neighboring *B. subtilis* cells.

Intercellular Nanotubes Connect Neighboring *B. subtilis* Cells

The exchange of cytoplasmic molecules between adjacent cells raised the notion that intercellular connections, facilitating this process, exist. To examine this possibility, we grew *B. subtilis* cells (PY79) on solid Luria Bertani (LB) medium and visualized

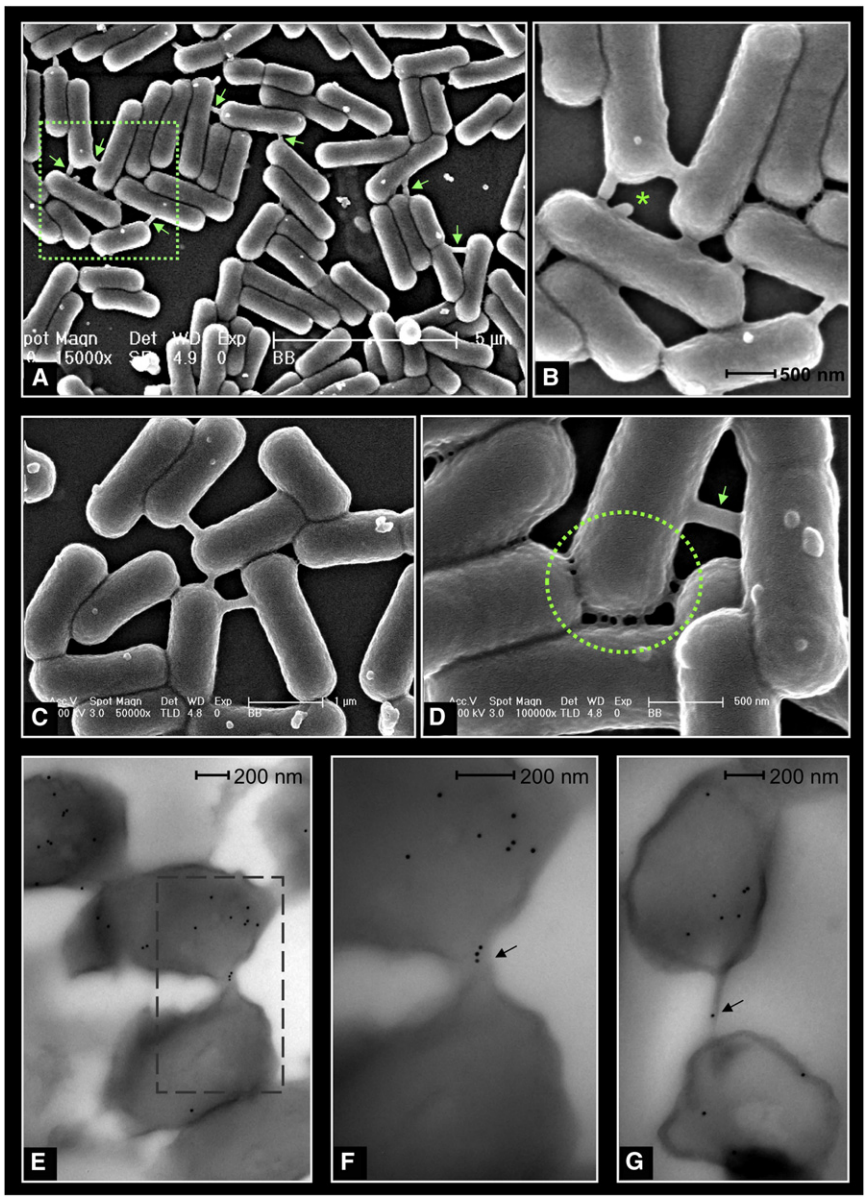

Figure 3. Intercellular Nanotubes Form between Neighboring *B. subtilis* Cells

(A–D) PY79 cells were grown to midexponential phase, plated on LB agar, incubated for 6 hr at 37°C, and visualized by HR-SEM (see Experimental Procedures). (A) A typical field of *B. subtilis* cells (×15,000). Green arrows indicate intercellular nanotubes connecting neighboring cells. The scale bar represents 5 μm. (B) A higher-magnification image (×40,000) of the boxed region in (A). Membrane bulging is indicated by an asterisk (*). The scale bar represents 500 nm. (C) An additional field of cells demonstrating the occurrence of a network of intercellular nanotubes (×50,000). The scale bar represents 1 μm. (D) A field of cells where a cluster of smaller nanotubes (highlighted by a dashed circle) as well as a more pronounced larger tube (indicated by an arrow) are apparent (×100,000). The scale bar represents 500 nm.

(E) An immuno-EM section of cocultured PY79 (*gfp*−) and SB444 (*gfp*+) cells, stained with anti-GFP and secondary gold-conjugated antibodies (see Extended Experimental Procedures). Black dots indicate the expression and localization of GFP molecules. The scale bar represents 200 nm.

(F) A magnification of the dashed square in (E). The arrow highlights the flow of GFP molecules within a tube. The scale bar represents 200 nm.

(G) An additional example of an immuno-EM section, showing the localization of a GFP molecule within a tube, as indicated by an arrow. The scale bar represents 200 nm.

See also Figures S4 and Figure S5.

them with high-resolution scanning electron microscopy (HR-SEM; see Experimental Procedures). Surprisingly, tubular protrusions (nanotubes) bridging neighboring cells were plainly visible (Figure 3A). The nanotubes seem to project from the cell surface at different positions in a nonspecific manner. Higher-magnification micrographs clearly evidence a network of intercellular connecting nanotubes whereby cells frequently attach to more than one partner simultaneously (Figures 3B and 3C and Figure S4A). Occasionally, we observed the occurrence of branched nanotubes linking together several cells at once (Figure S4B). Notably, these tubes were structurally distinguishable from classical conjugative pili (Figure S4C). Examining cells of an undomesticated *B. subtilis* strain (3610) with the same procedure revealed a similar or an even enhanced ability to form nanotubes (Figure S4D). The existence of nanotubes was also detected when cells were incubated on minimal medium yet at a lower frequency (Figure S4G). However, nanotubes seem to be absent when cells were grown in liquid medium (data not shown), suggesting that growth on solid medium induces their formation.

Tube dimension appears to vary with the distance between connected cells. Generally, tube length ranged up to 1 μm, whereas width ranged approximately from 30 to 130 nm (e.g., Figures S4E and S4F). The relatively large size of the tubes concords with our assumption that they could easily accommodate the passage of proteins such as GFP (approximately 40 Å; [Yang et al., 1996]) and even larger cytoplasmic molecules. Closer investigation of the HR-SEM images revealed that beside the large nanotubes, an additional type of smaller nanotubes was visible, though more challenging to detect (Figure 3D). These smaller tubes tended to be clustered connecting nearby cells intimately, appearing to actually "stitch" one cell to another. We speculate that these smaller nanotubes are more ubiquitous than the larger ones and are capable of traversing small molecules.

In an alternative approach, intercellular connections were visualized with transmission electron microscopy (TEM), where cells were imaged without employing any contrasting agent

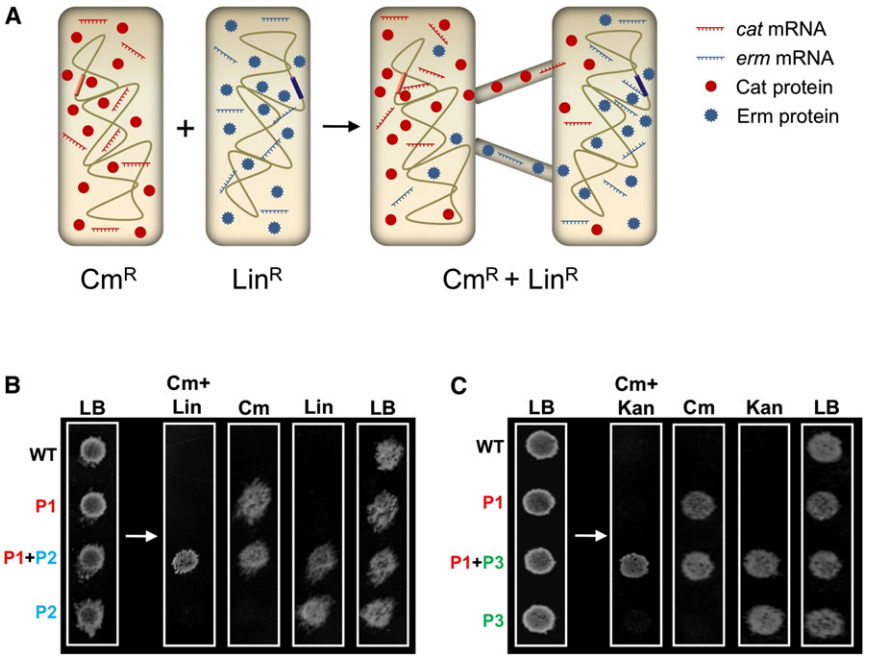

Figure 4. Transient Nonhereditary Phenotypes Can Be Acquired from Neighboring Cells

(A) A schematic model for the transient gain of nonhereditary phenotypes via intercellular nanotubes. Shown on the left are two *B. subtilis* cells, each harboring a different antibiotic resistance gene, providing Cm^R or Lin^R. Genes (colored stripes) are depicted on the chromosomes (olive lines) with colored circles and colored combs indicating their respective proteins and transcripts. Shown on the right is the gain of antibiotic resistance by proteins and transcripts passing through intercellular nanotubes in a mixed population. Molecular transfer through the connecting tubes yields a population of cells temporarily resistant to both antibiotics in a nonhereditary fashion.

(B) An antibiotic assay examining the exchange of Cat and Erm proteins (and possibly transcripts) between two different *B. subtilis* strains. Left: Equal numbers of cells from PY79 (WT), SB463 (*amyE::*$P_{hyper\text{-}spank}$*-cat-spec*) (P1: Cm^R), and GD57 (*amyE::*$P_{hyper\text{-}spank}$*-erm-spec*) (P2: Lin^R) strains were spotted separately on LB agar. In parallel, equal numbers of mixed P1 and P2 cells (1:1) were spotted similarly. Cells were grown for 4 hr at 37°C. Right: Grown cells were replica plated onto the indicated selective plates and finally onto LB. Plates were incubated O/N at 37°C.

(C) An antibiotic assay examining the exchange of Cat and Kan resistance proteins (and possibly transcripts) between two different *B. subtilis* strains. Left: Equal numbers of cells from PY79 (WT), SB463 (*amyE::*$P_{hyper\text{-}spank}$*-cat-spec*) (P1: Cm^R), and SB513 (*amyE::*$P_{hyper\text{-}spank}$*-gfp-kan*) (P3: Kan^R) strains were spotted separately on LB agar. In parallel, equal numbers of mixed P1 and P3 cells (1:1) were spotted similarly. Spotted cells were grown for 4 hr at 37°C. Right: Grown cells were replica plated onto the indicated selective plates and finally onto LB. Plates were incubated O/N at 37°C.
See also Figure S6 and Figure S7.

(see Extended Experimental Procedures). Consistent with the HR-SEM images, a network of pronounced nanotubes tying one cell to another was readily visible (Figure S5A). Interestingly, higher-magnification analysis of a typical tube appears to indicate a structure comprising outer and inner layers, hinting at a multilayered structure (Figures S5B–S5D). Moreover, thin section analysis suggests that the tubes contain cell wall material, membrane and cytoplasmic content (Figures S5E and S5F).

To demonstrate that nanotubes indeed serve as a route for trading cytoplasmic molecules, we carried out immunoelectron microscopy (immuno-EM). *gfp*+ and *gfp*− cells were mixed and grown on solid medium. Next, cells were gently fixed, sectioned, incubated with anti-GFP antibodies and then immunostained with gold-conjugated secondary antibodies (see Extended Experimental Procedures). Remarkably, the gold particles could be visualized within nanotubes connecting neighboring cells (Figures 3E–3G), corroborating that indeed intercellular nanotubes serve as a path for molecular exchange. In many images, a GFP gradient was observed whereby a GFP-producing cell containing multiple gold particles was connected to an adjacent cell containing few gold particles (Figure 3E), resembling the phenomenon observed by time-lapse microscopy (Figure 1C). Importantly, when only *gfp*− cells were similarly processed, no significant gold signal was detected (data not shown).

Thus, intercellular nanotubes bridge adjacent *B. subtilis* cells, thereby generating a network of tubular conduits that enable the exchange of cytoplasmic content.

Transient Nonhereditary Resistance to Antibiotics Can Be Acquired from Adjacent Cells

Having established the existence of intercellular nanotube networks, we sought to explore their capability to generate new phenotypes. We anticipated that when two strains, each harboring a different antibiotic resistance gene, are grown together, the exchange of cytoplasmic molecules (proteins and possibly transcripts) through the tubes could yield a population of cells temporarily resistant to both antibiotics in a nonhereditary fashion (Figure 4A).

To test this prediction, we examined the exchange of chloramphenicol acetyltransferase (Cat) and erythromycin resistance methylase (Erm) between two different *B. subtilis* strains. The Cat protein confers resistance to chloramphenicol (Cm) and the Erm protein confers resistance to lincomycin (Lin). Strains harboring chromosomally encoded resistance to Cm (P1: Cm^R) or Lin (P2: Lin^R) were spotted separately or in a mixture onto LB agar plate and incubated for 4 hr in the absence of any antibiotic selection. Next, the ability of the strains to grow on selective plates containing Cm, Lin, or both was examined by replica plating (Figure 4B) in order to maintain the spatial arrangement of the cells. Strikingly, the mixed population of P1 and P2 cells was able to survive on the antibiotic plate containing both Cm and Lin (Figure 4B). To explore the genotype of the survivors, cells growing on the Cm+Lin plate were streaked onto a nonselective LB plate. Then individual colonies from the streak were picked, grown as stripes on LB plates, and their genotype was

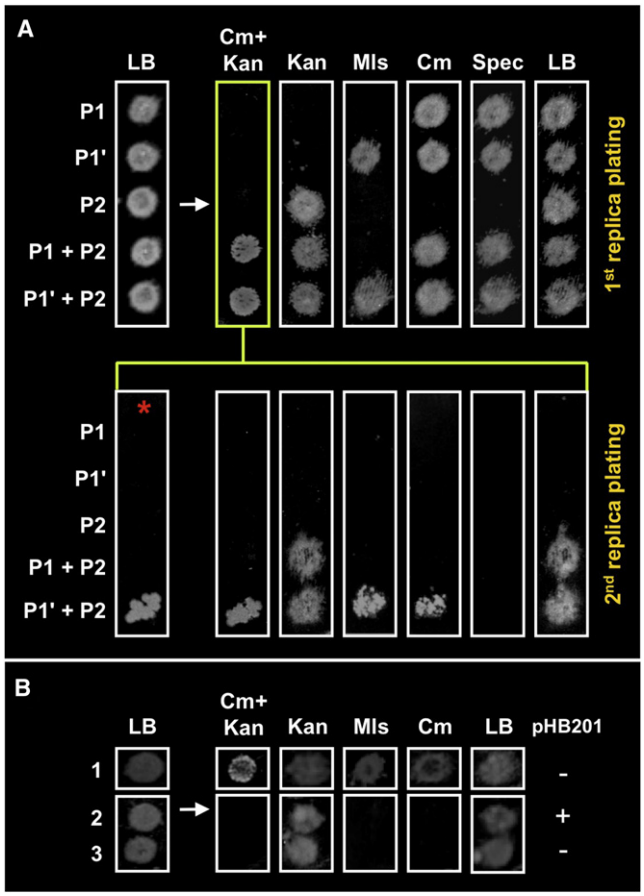

Figure 5. Plasmids Can Be Transferred between Neighboring Cells

(A) An antibiotic assay examining the transfer of plasmids between *B. subtilis* cells. Left: Equal numbers of cells from P1 (SB463: *amyE::P*$_{hyper\text{-}spank}$*-cat-spec*) (Cm^R, Spec^R), P1′ (GD110: *amyE::P*$_{hyper\text{-}spank}$*-cat-spec*, pHB201/*cat, erm*) (Cm^R, Spec^R, Mls^R), and P2 (SB513: *amyE::P*$_{hyper\text{-}spank}$*-gfp-kan*) (Kan^R) strains were spotted separately on LB agar. In parallel, equal numbers of mixed P1+P2 (1:1) and mixed P1′+P2 (1:1) cells were spotted similarly. Cells were grown for 4 hr at 37°C. Right: Grown cells were replica plated onto the indicated plates (first-replica plating), and plates were incubated O/N at 37°C. Lower: To analyze the genotype of the cells growing on Cm+Kan antibiotic plate (highlighted with a green frame) cells were re-replica plated onto the indicated plates (second-replica plating). The plate labeled with an asterisk contains Cm+Kan+Mls. Plates were incubated O/N at 37°C.

(B) An antibiotic assay demonstrating that the plasmid is not transmitted by transformation. Left: (1) A mixture of GD110 (*amyE::P*$_{hyper\text{-}spank}$*-cat-spec*, pHB201/*cat, erm*) (Cm^R, Spec^R, Erm^R) and SB513 (*amyE::P*$_{hyper\text{-}spank}$*-gfp-kan*) (Kan^R) cells. (2–3) SB513 cells. Spotted cells were grown for 4 hr at 37°C in the presence or the absence of exogenous pHB201 DNA (100 ng of DNA/μl spotted cells) as indicated. Right: Grown cells were replica plated onto the indicated plates and incubated O/N at 37°C.

determined by replica plating onto Cm and Lin plates (Figure S6A). Each tested colony exhibited either Cm^R or Lin^R, but not both, indicating that the surviving cells have not acquired a doubly resistant genotype. Summarily, we infer that nearby cells can exchange cytoplasmic molecules and gain transient nonhereditary phenotypes.

Both Cm and Lin are bacteriostatic antibiotics that impede growth but do not instantly kill bacterial cells. On the other hand, bactericidal antibiotics kill bacteria rapidly, and thus necessitate constant protection by the resistance protein. Therefore, it remained possible that the dual resistance obtained by the mixed population would be affected if one of the participants harbors a gene imparting resistance to a bactericidal antibiotic. To examine this premise, we cocultured P1 strain (Cm^R) with P3 strain harboring chromosomally encoded resistance to the bactericidal antibiotic Kanamycin (Kan^R) and repeated the above assay (Figure 4C). In line with previous results, only cells in the mixed population were able to grow on the antibiotic plate containing both Cm and Kan (Figure 4C). Genotypic analysis of the surviving cells revealed that they were exclusively Kan^R Cm^S, implying that the P3 cells carrying the bactericidal antibiotic resistance gene survived (Figure S6B). Expanding this genotypic examination to thousands of colonies revealed that Cm^R cells (P1) survive rarely (~1:700) under these conditions. This assay enables delineation between "donor" (Cm^R) and "recipient" (Kan^R) strains, providing an approach to follow the directionality of molecular exchange. To further confirm that the doubly resistant P3 cells indeed acquired Cat molecules from their neighbors, we carried out immunofluorescence microscopy with anti-Cat antibodies to detect the presence of Cat protein molecules within their cytoplasm (see Extended Experimental Procedures). Consistent with our assumption, a clear fluorescent signal was detected from P3 cells grown in the mixture but was evidently absent from unmixed P3 cells (Figure S6C).

Taken together, we conclude that the transient doubly resistant phenotype is a nonhereditary feature, and the resulting survivors are affected by the mechanism of antibiotic action.

Plasmids Can Be Traded between Neighboring Cells

Given that nonhereditary features can be traded between nearby cells, we explored whether genetic information carried by an extrachromosomal plasmid can also be exchanged. To examine this possibility, we transformed *B. subtilis* strain P1 (SB463: *amyE::P*$_{hyper\text{-}spank}$*-cat-spec*) (Cm^R, Spec^R) with a nonintegrative vector pHB201 (6.6 kb ~4.35 MDa; *cat, erm*) (Cm^R, Mls^R) (Bron et al., 1998). The resultant strain P1′ (GD110) was consequently Cm^R, Spec^R, and Mls^R (Mls is a mixture of Erm and Lin, both can be neutralized by *erm*). Next, P1 and P1′ were spotted separately or in a mixture with P2 strain (SB513: *amyE::P*$_{hyper\text{-}spank}$*-gfp-kan*) (Kan^R, GFP+) on a nonselective plate, grown for 4 hr, and the antibiotic resistance of these populations was tested (Figure 5A). Consistent with previous results, only cells within the mixed cultures (P1+P2 or P1′+P2) were able to grow on a plate containing both Cm and Kan (Figure 5A, first-replica plating). To distinguish exchange of nonhereditary molecules from plasmid delivery, we examined whether the observed dual resistance was heritable. Accordingly, cells growing on Cm+Kan were re-replica plated onto respective antibiotic plates to determine their genotype (Figure 5A, second-replica plating). In line with the data described above, cells from the P1+P2 mixture did not resume growth on the Cm+Kan plate but were able to grow on the Kan plate, implying that their dual resistance was a transient nonhereditary feature exhibited by recipient P2 cells. In contrast, a substantial fraction of the P1′+P2 population grew on the Cm+Kan plate and also on a plate containing Cm+Kan+Mls

(Figure 5A, asterisk). The emergence of cells carrying Kan, Cm, and Mls resistances suggests that the plasmid pHB201 (Cm^R, Mls^R) was transferred from the donor P1′ (Kan^S) strain to the recipient P2 (Kan^R) strain. Indeed, these multiply resistant cells were all $Spec^S$ and GFP+, supporting the view that P2 ($Spec^S$, GFP+) rather than P1′ ($Spec^R$, GFP−) cells survived (Figure 5A, second-replica plating; data not shown). Finally, pHB201 could be extracted from the multiply resistant cells confirming that their phenotype was not a consequence of genetic mutations but derived from receipt of the extrachromosomal plasmid (data not shown).

To substantiate that the plasmid was not delivered to recipient cells by transformation, P2 cells were incubated with an excess amount of exogenous pHB201 DNA. Exogenous addition of plasmid DNA was unable to allow growth of P2 cells on the Cm+Kan plate, indicating that transformation is not the mechanism for plasmid exchange under our experimental conditions (Figure 5B). Furthermore, plasmid transfer was DNaseI resistant (see Extended Experimental Procedures and data not shown), implying that the transferred DNA is protected during passage from one cell to another by nanotubes that serve as a delivery vehicle. Similarly, DNaseI resistance was found to be a characteristic of conjugative plasmids passing through the protective conjugative tube (Koehler and Thorne, 1987). Measuring the frequency of pHB201 transfer revealed a value of 10^{-7}/colony forming unit (CFU) (see Extended Experimental Procedures). In comparison, examining the transfer of a bona fide conjugative plasmid (pLS20) revealed a transfer frequency that was 1000 fold higher than pHB201 (10^{-4}/CFU), similar to the frequencies reported previously (Koehler and Thorne, 1987; Tanaka and Koshikawa, 1977).

We conclude that when grown on solid surface, *B. subtilis* cells are able to exchange nonconjugative plasmids. Unlike conjugation, which is induced by genes carried on conjugative plasmids, intercellular nanotubes may provide a constitutive path for reciprocal genetic exchange in nature without the need for a donor or a recipient strain.

Investigating the Nature of Nanotubes

Next, we asked if, similar to their eukaryotic counterparts and as indicated by our TEM analysis, bacterial nanotubes are indeed composed of membrane constituents (Belting and Wittrup, 2008; Hurtig et al., 2010; Schara et al., 2009; Figure S5). To explore this possibility, we examined nanotubes sensitivity to the membrane detergent sodium dodecyl sulfate (SDS). Initially, we tested whether SDS influences the phenomenon of acquiring nonhereditary antibiotic resistance from neighboring cells. Hence, cocultured P1 (Cm^R) and P2 (Kan^R) cells were spotted onto LB plates containing different concentrations of SDS, and their ability to grow on Cm+Kan plates was assayed by replica plating. An inverse correlation was observed between growth of the mixed cells on the Cm+Kan plate and SDS concentration (Figure S7A). Importantly, at a concentration of 0.009% SDS, the ability of the cells to grow on the Cm+Kan selective plate was abolished, yet their viability was not significantly affected (Figure S7B). These results show that SDS prevents acquisition of antibiotic resistance from nearby cells, suggesting bacterial nanotubes are SDS sensitive.

To examine the SDS sensitivity of nanotubes, cells grown in the presence of SDS were visualized with HR-SEM. Indeed, when we observed cells growing at 0.007% SDS, a concentration in which acquiring antibiotic resistance was clearly decreased (Figure S7A), only few intercellular nanotubes could be discerned (Figure S7C). However, prominent nanotubes were evident in untreated cells (Figure S7D). These SDS experiments indicate that nanotubes are composed of membrane components and further correlate the integrity of nanotubes with the exchange of antibiotic resistance among neighbors.

We exploited the antibiotic resistance assay to screen for bacterial genes that influence nanotube formation. Specifically, we analyzed an array of mutants in cell division, cell shape and membrane metabolism for their capacity to exchange antibiotic resistance (Table S1). However, none of the tested mutants significantly reduced the antibiotic resistance of the mixed population. It is possible that nanotube production is induced by several overlapping mechanisms involving different gene families in a cooperative manner.

Intercellular Nanotubes Form between Different Bacterial Species

To broaden our investigation, we examined whether the exchange of cytoplasmic molecules and the formation of intercellular nanotubes occur between species. First, we investigated the ability of *B. subtilis* cells to transfer cytoplasmic molecules to the Gram-positive coccus, *Staphylococcus aureus*. *B. subtilis* (*gfp*+) and *S. aureus* (*gfp*−) cells were cocultured and followed by time-lapse fluorescence microscopy. Remarkably, at t30 min, a significant fluorescence signal was acquired by the *S. aureus* cells in a manner proportional to their distance from the *gfp*+ *bacilli* cells (Figure 6A). This phenomenon was reinforced after 50 min of coincubation (Figure 6A and Figure S3Bb). We surmise that molecular transfer can take place between two distinct species of Gram-positive bacteria that reside in proximity.

Examining a field of cocultured cells by HR-SEM revealed visible intercellular bridges among the cells of each species, but, more importantly, clear protrusions were formed between species (Figure 6B). Visualizing the intercellular nanotubes formed between *S. aureus* cells in high resolution revealed morphology and dimensions similar to the large tubes formed by *B. subtilis* cells (Figure 6C). The interspecies *B. subtilis*-*S. aureus* connections also displayed morphology resembling that of *B. subtilis* nanotubes (Figure 6D and Figure S4H). We infer that Gram-positive bacteria can trade cellular information within and between species by a path comprising of the intercellular connections.

Finally, we addressed whether cytoplasmic molecules can be traded between evolutionary distant Gram-positive and -negative bacteria. We therefore tested the capability of *B. subtilis* cells to transfer cytoplasmic molecules to the Gram-negative bacterium *Escherichia coli*. When *B. subtilis* (*gfp*+) cells were cultured alongside *E. coli* (*gfp*−) cells, a pronounced fluorescence gradient developed in a temporal manner (Figure 7A and Figure S3Bc). Accordingly, interspecies nanotubes directly bridging neighboring *B. subtilis* and *E. coli* cells were evident by HR-SEM (Figures 7B and 7C). In general, the nanotubes formed by *E. coli*

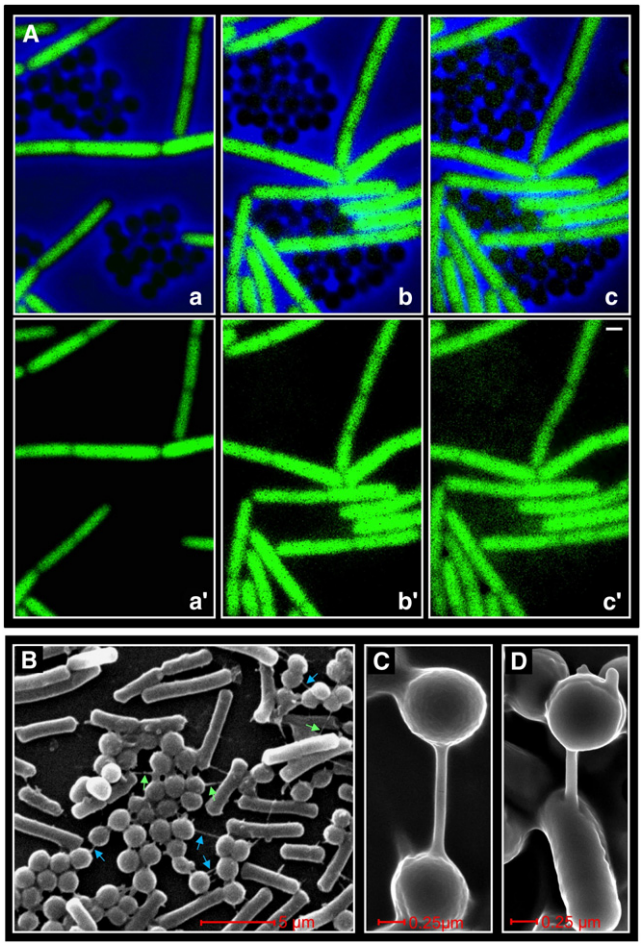

Figure 6. Interspecies Nanotubes Connecting *B. subtilis* and *S. aureus* Cells

(A) Exponentially growing cells of *B. subtilis* SB444 (*gfp*+) and *S. aureus* (MRSA) (*gfp*−) strains were mixed (1:1 ratio), plated on an LB agarose pad, and incubated in a temperature controlled chamber at 37°C. Cells were visualized by time-lapse fluorescence microscopy, and images of phase contrast (blue) and fluorescence (green) were collected at 10 min intervals. Select overlay (a–c) and GFP (a′–c′) images are shown from the following time points: (a and a′) t0 min (b and b′) t30 min and (c and c′) t50 min. The scale bar represents 1 μm. (B–D) *B. subtilis* (PY79) and *S. aureus* (MRSA) cells were grown to mid-exponential phase. Grown cells were mixed (1:1 ratio), plated on LB agar, incubated for 6 hr at 37°C, and visualized by HR-SEM (see Experimental Procedures). (B) A typical field of the mixed population (×12,000). Blue arrows indicate visible intercellular nanotubes between *S. aureus* cells, whereas green arrows point to interspecies *B. subtilis* and *S. aureus* connecting tubes. (C) A high-magnification image (×50,000) of a nanotube connecting two *S. aureus* cells. (D) A high-magnification image (×50,000) of an interspecies nanotube connecting *S. aureus* and *B. subtilis* cells. The scale bars represent 5 μm (B) and 0.25 μm (C and D).

See also Figure S3 and Figure S4.

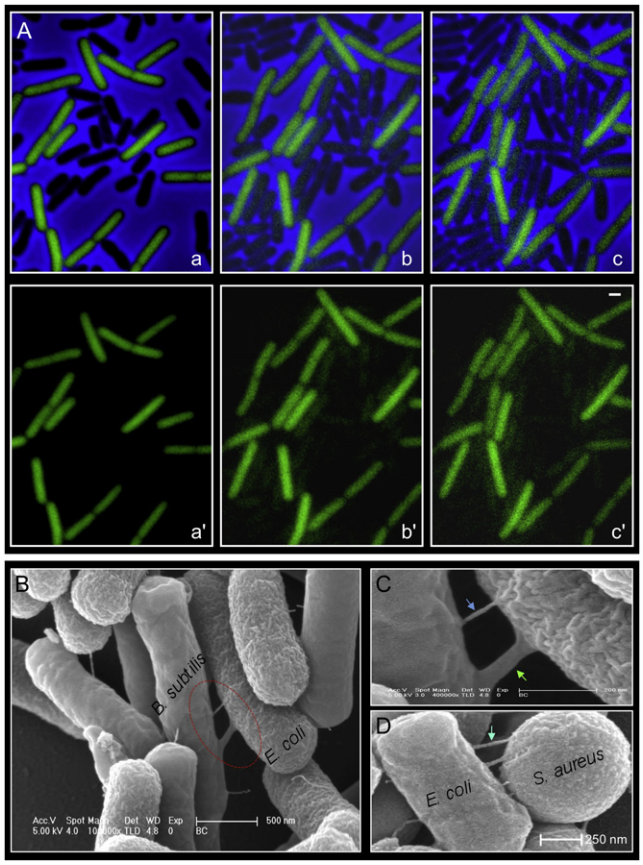

Figure 7. Interspecies Nanotubes Form between Gram-Positive and -Negative Bacteria

(A) Exponentially growing cells of *B. subtilis* SB444 (*gfp*+) and *E. coli* (MG1655) (*gfp*−) strains were mixed (1:1 ratio), plated on an LB agarose pad, and incubated in a temperature controlled chamber at 37°C. Cells were visualized by time-lapse fluorescence microscopy, and images of phase contrast (blue) and fluorescence (green) were collected at 10 min intervals. Select overlay (a–c) and GFP (a′–c′) images are shown from the following time points: (a and a′) t0 min (b and b′), t30 min, and (c and c′) t50 min. The scale bar represents 1 μm. (B and C) *B. subtilis* (PY79) and *E. coli* (MG1655) cells were grown to mid-exponential phase. Grown cells were mixed (1:1 ratio), plated on LB agar, incubated for 6 hr at 37°C, and visualized by HR-SEM (see Experimental Procedures). (B) A typical field of the mixed population (×100,000) is shown. The red circle highlights nanotubes between neighboring *B. subtilis* and *E. coli* cells. (C) A higher-magnification image (×400,000) of the circled region in (B). Based on texture similarity, the green arrow denotes a thick nanotube emanating from the *B. subtilis* cell and the blue arrow indicates a thinner nanotube emanating from the *E. coli* cell. The scale bars represent 500 nm (B) and 200 nm (C).

(D) *S. aureus* (MRSA) and *E. coli* (MG1655) cells were grown to midexponential phase. Grown cells were mixed (1:1 ratio), plated on LB agar, incubated for 6 hr at 37°C, and visualized by HR-SEM (×75,000). An arrow indicates interspecies tubes connecting two neighboring cells. The scale bar represents 250 nm.

See also Figure S3.

cells appeared significantly thinner than those formed by *B. subtilis* or *S. aureus,* suggesting that Gram-positive and -negative bacteria form somewhat different types of nanotubes. HR-SEM also clearly revealed the presence of nanotubes formed between *S. aureus* and *E. coli* (Figure 7D) demonstrating the ubiquitous nature of this phenomenon.

DISCUSSION

We revealed the existence of a previously unidentified form of bacterial communication that facilitates the exchange of cytoplasmic constituents between adjacent cells via intercellular

connecting tubes. Utilizing microscopy and genetic assays, we show that small cytoplasmic molecules and proteins can be traded between cells grown in proximity, thereby generating transient, nonheritable traits. Moreover, we demonstrate that nonconjugative plasmids can be transferred from one cell to another, resulting in transmission of hereditary features to recipient cells. Our data support that this type of communication is mediated by tubular projections that bridge neighboring cells and create a syncytium-like multicellular consortium. We propose that nanotube-mediated cytoplasmic sharing represents a key form of intercellular bacterial communication in nature, providing an efficient path for trading intracellular molecules between species. This attribute allows the emergence of new phenotypes by multispecies bacterial communities, increasing their survival in fluctuating environments.

To date, the best characterized form of intercellular bacterial communication is known to be mediated by extracellular signaling molecules (Bassler and Losick, 2006; Lazazzera, 2001; Ng and Bassler, 2009). This type of communication is, however, constrained by the ability of bacteria to secrete and/or recognize the signal, transduce the received information, and modulate gene expression correspondingly. In contrast, communicating by nanotubes enables bacteria a straightforward immediate transfer of information that can cross the inherent species barrier. Moreover, because tunnels presumably maintain inner-cellular physiological conditions, channeled molecules are potentially protected from degrading enzymes and harsh environmental conditions. Taken together, nanotube-mediated informational flow is potentially both continuous and efficient and, as we show here, can enable molecular transfer across long distances in bacteria grown on solid surfaces (Figures 1A and 1B).

Intercellular nanotubes connecting bacterial cells have been observed during conjugation, which is induced by conjugative plasmids and occurs in a unidirectional fashion from donor to recipient (Madigan et al., 2003). In contrast, the plasmid transfer described here does not require any intrinsic plasmid elements, and a given cell can be either donor or recipient. A similar phenomenon has been previously observed in archaebacteria, where nonconjugative plasmids were shown to reciprocally traverse from one cell to another and cytoplasmic bridges were detected between cells (Rosenshine et al., 1989; Schleper et al., 1995). Therefore, nanotube-mediated plasmid transfer in bacteria, though less efficient than classical conjugation, most likely represents a more ubiquitous form of horizontal gene transfer in nature, enabling universal interspecies plasmid exchange without the need for a dedicated mechanism.

Establishing nanotube networks may represent a central mode of intercellular communication of biofilm inhabitants, typically composed of various species lying in proximity in a defined space (Kolter and Greenberg, 2006; Kuchma and O'Toole, 2000; Lemon et al., 2008; Straight and Kolter, 2009). We speculate that the syncytium-like synergistic consortium created by nanotubes mediates trading of valuable molecules, enabling biofilm occupants to gain new traits and enhances the overall population fitness. Accordingly, cooperation between different bacterial species in a biofilm underlies development of novel communal features such as synergistic degradation of complex molecules (e.g., Christensen et al., 2002; Moons et al., 2009). Intercellular nanotubes could also play a role in other social activities. For instance, the formation of multicellular fruiting body by the bacterium *Myxococcus xanthus* requires a coordinated gliding motility (Kaiser, 2008; Kearns and Shimkets, 2001) that may be promoted by cell-to-cell contact. Interestingly, motility-associated outer-membrane lipoproteins can be readily exchanged between *M. xanthus* cells (Nudleman et al., 2005). Another intriguing social activity is the ability of certain wild strains of *E. coli* to inhibit growth of laboratory strains by contact-dependent mechanism (Aoki et al., 2005). It is possible that the need for physical cell-to-cell attachment to facilitate this action is driven by conduits that allow the transfer of inhibitory factors. Therefore, nanotubes may provide an efficient strategy to fight against competitors by the delivery of toxic molecules to neighboring cells.

The bacterial nanotubes observed in this study can be broadly categorized into two types: (1) thick tubes connecting more distal cells and (2) thin tubes present in arrays that connect nearby cells in a more intimate manner (Figure 3). Plausibly, the thinner tubes support the flow of small molecules, such as nutrients, relatively short proteins, and transcripts, whereas the thicker nanotubes accommodate larger cargo, such as protein complexes and supercoiled plasmids. Interestingly, F pili that allow the transfer of a single-stranded DNA have an outside diameter of approximately 8 nm (Madigan et al., 2003; Silverman, 1997; Figure S4C), which is significantly thinner than that of larger nanotubes observed here. In mammalian cells, diverse-sized nanotubes are formed frequently by a wide variety of cell types and have been shown to deliver small substances, proteins, membrane vesicles, and even to provide a route for the spread of prions and viruses such as HIV (Davis and Sowinski, 2008; Hurtig et al., 2010; Sherer et al., 2007). By analogy, it is conceivable that bacterial nanotubes could provide a conduit for bacteriophages and their components (such as DNA) to spread from one cell to another. In this regard, the diameter of phage lambda is 55 nm (Hershey and Dove, 1983), whereas the nanotube width we observed was frequently larger than 100 nm.

The molecular composition of bacterial nanotubes remains to be resolved, though their SDS sensitivity and electron microscopy (EM) analyses evidence that they are arranged in a multilayered structure composed of cell wall material, membrane components, and cytoplasmic content (Figures S5B–S5F and Figure S7). The texture of the nanotubes (e.g., Figure 7) highly resembles the bacterial cell surface, suggesting similar exterior composition and surface continuity. Notably, initiation of nanotube formation sometimes appeared in our EM images as bulging of the cell surface (Figure 3B and Figure S5F). It is conceivable that these protrusions are initiated by local lysis of the cell wall that triggers membrane bulging, especially in Gram-positive bacteria that are encased by a thick cell wall. In Gram-negative bacteria, nanotubes may emanate from, or connect with, the outer membrane, as shown for membrane vesicle production (Mashburn-Warren and Whiteley, 2006). In this way, the delivered molecules should cross the additional barrier of the plasma membrane. The formation of nanotubes between evolutionary distinct species raises the possibility that

attachment involves general mechanisms of membrane fusion and curvature (Martens and McMahon, 2008). However, it is also possible that bacterial nanotubes assemble and function in a similar manner to the secretion systems (type III, IV, and VI) of pathogenic Gram-negative bacteria, utilized for establishing interaction with their host cells (Tseng et al., 2009).

Many questions remain unanswered concerning how cargo is transported through nanotubes. We do not know whether the transport is active and requires energy or is passive and prompted by diffusion. It is possible that both mechanisms coexist and utilization depends on the delivered cargo. In eukaryotic cells, nanotubes are frequently associated with cytoskeletal and motor proteins, implying a role for active transport (Davis and Sowinski, 2008). The directionality of the transport is also elusive and raises the following questions: is there a defined donor and recipient, and does directionality depend on the cell that initiates tube formation? It will be interesting to explore whether a gating mechanism exists to control traffic directionality.

Our discovery that diverse bacterial species can communicate with nanotubes has significant medical implications. As we have demonstrated, both hereditary and nonhereditary antibiotic resistance can be acquired from neighboring cells through nanotubes, a survival strategy that could be widespread in nature. This unhampered informational flow raises the concern that nanotubes allow commensal bacteria to nurture pathogenic bacteria. Conversely, pathogenic bacteria may transfer virulence features to commensal bacteria converting them into pathogens. In this view, gaining a better molecular understanding of nanotube formation could lead to the development of novel strategies to fight against pathogenic bacteria.

EXPERIMENTAL PROCEDURES

Strains and Plasmids

B. subtilis strains used in this study are derivatives of the wild-type PY79 strain and listed in Table S2. The undomesticated *B. subtilis* strain NCIB 3610 was used when indicated. The *E. coli* strain used was K12-MG1655 and the *S. aureus* strain was MRSA (Mulligan et al., 1993). Plasmid constructions are described in Table S3 and primers are listed in Table S4.

General Methods

Cells were grown in LB or in S7 minimal medium at the indicated temperature. Cultures were inoculated at an OD_{600} of 0.05 from an overnight (O/N) culture. Induction of $P_{hyper\text{-}spank}$ promoter was carried out by adding isopropyl β-D-1-thiogalactopyranoside (IPTG) to a final concentration of 1 mM. Antibiotics were used at the following concentrations: Kan 6 μg/ml, Cm 6 μg/ml, Lin 70 μg/ml, Erm 1 μg/ml, and Spec 100 μg/ml. Other general methods were carried out as described previously (Harwood and Cutting, 1990).

Fluorescence Microscopy

Fluorescence microscopy was carried out as described previously (Bejerano-Sagie et al., 2006). For time-lapse microscopy observations, a mounting frame (A-7816, Invitrogen) was filled with 1% LB agarose with or without 1 mM IPTG. Cells were grown to midexponential phase, and samples (0.5 ml) were removed, centrifuged briefly, and spotted on the agarose pad. Cells were incubated in a temperature-controlled chamber (Pecon-Zeiss, Germany) and visualized and photographed with Axio Observer Z1 (Zeiss, Germany), equipped with CoolSnap HQII camera (Photometrics, Roper Scientific, USA). System control and image processing were performed with MetaMorph 7.4 software (Molecular Devices, USA). Additional fluorescence microscopy methods are described in Extended Experimental Procedures.

HR-SEM Analysis

Exponentially growing *B. subtilis, E. coli*, or *S. aureus* cells were plated on LB or S7 agar, either separately or in a mixture, as indicated. Cells were incubated for 3 hr at 37°C and then EM grids (FCF300-Cu, EMS, USA) were placed on top of the growing cells. Plates were incubated for additional 3 hr and EM grids were removed gently. Cells attached to the grids were washed with 0.1 M sodium cacodylate buffer ($Na\ (CH_3)_2\ AsO_2 \cdot 3H_2O$) (pH 7.2) and then fixed with 2% glutaraldehyde in sodium cacodylate buffer (0.1 M, [pH 7.2]) for 2 hr at 25°C. Next, cells were postfixed by incubation with 1% osmium tetroxide for 1 hr at 25°C in the dark and then dehydrated by exposure to a graded series of ethanol washes [25%, 50%, 75%, 95%, and 100% (×2); 10 min each]. Finally, the grid-attached cells were washed with a graded series of freon 113 (25%, 50%, 75%, 95%, and 100% freon in ethanol; 10 min each). Specimens were coated with gold-palladium (~8 nm cluster size) with Quorum Technologies SC7640 Sputter Coater and cells observed with a FEG HR-SEM (Sirion [FEI]). Additional EM procedures are described in Extended Experimental Procedures.

SUPPLEMENTAL INFORMATION

Supplemental Information includes Extended Experimental Procedures, seven figures, and four tables, and can be found with this article online at doi:10.1016/j.cell.2011.01.015.

ACKNOWLEDGMENTS

We thank I. Popov, E. Blayvas, N. Feinstein, and E. Rahamim (Hebrew University, IL) for technical support during EM studies. We are grateful to A. Rouvinski (Hebrew University, IL) for experimental advice and insightful discussions. We thank R. Losick (Harvard University, USA), M. Kassel (National Institutes of Health, USA), G. Bachrach (Hebrew University, IL), D. Kearns (Indiana University, USA), A. Taraboulos (Hebrew University, IL), and members of the Ben-Yehuda laboratory for valuable discussions and comments. We thank the National BioResource Project National Institute of Genetics, Japan (NIG, Japan) for providing *B. subtilis* mutant strains. This work was supported by the European Research Council Starting Grant (209130), and by the Israel Science Foundation (696/07) awarded to S. B-Y.

Received: June 8, 2010
Revised: October 18, 2010
Accepted: January 10, 2011
Published: February 17, 2011

REFERENCES

Aoki, S.K., Pamma, R., Hernday, A.D., Bickham, J.E., Braaten, B.A., and Low, D.A. (2005). Contact-dependent inhibition of growth in *Escherichia coli*. Science *309*, 1245–1248.

Bassler, B.L., and Losick, R. (2006). Bacterially speaking. Cell *125*, 237–246.

Bejerano-Sagie, M., Oppenheimer-Shaanan, Y., Berlatzky, I., Rouvinski, A., Meyerovich, M., and Ben-Yehuda, S. (2006). A checkpoint protein that scans the chromosome for damage at the start of sporulation in *Bacillus subtilis*. Cell *125*, 679–690.

Belting, M., and Wittrup, A. (2008). Nanotubes, exosomes, and nucleic acid-binding peptides provide novel mechanisms of intercellular communication in eukaryotic cells: implications in health and disease. J. Cell Biol. *183*, 1187–1191.

Bron, S., Bolhuis, A., Tjalsma, H., Holsappel, S., Venema, G., and van Dijl, J.M. (1998). Protein secretion and possible roles for multiple signal peptidases for precursor processing in *bacilli*. J. Biotechnol. *64*, 3–13.

Christensen, B.B., Haagensen, J.A., Heydorn, A., and Molin, S. (2002). Metabolic commensalism and competition in a two-species microbial consortium. Appl. Environ. Microbiol. *68*, 2495–2502.

Davis, D.M., and Sowinski, S. (2008). Membrane nanotubes: dynamic long-distance connections between animal cells. Nat. Rev. Mol. Cell Biol. *9*, 431–436.

Fuqua, C., and Greenberg, E.P. (2002). Listening in on bacteria: acyl-homoserine lactone signalling. Nat. Rev. Mol. Cell Biol. *3*, 685–695.

Giddings, T., and Staehelin, L.A. (1981). Observation of microplasmodesmata in both heterocyst-forming and non-heterocyst forming filamentous cyanobacteria by freeze-fracture electron microscopy. Arch. Microbiol. *129*, 295–298.

Golden, J.W., and Yoon, H.S. (2003). Heterocyst development in Anabaena. Curr. Opin. Microbiol. *6*, 557–563.

Harwood, C.R., and Cutting, S.M. (1990). Molecular biological methods for *Bacillus* (Chichester, New York: Wiley).

Haugland, R.P. (2005). Handbook-a Guidebook to Fluorescent Probes and Labelling Technologies (Carlsbad, CA, USA: Invitrogen Corp).

Heinlein, M., and Epel, B.L. (2004). Macromolecular transport and signaling through plasmodesmata. Int. Rev. Cytol. *235*, 93–102.

Hershey, A.D., and Dove, W. (1983). Lambda II (USA: New York, The Cold Spring Harbor Laboratory).

Hurtig, J., Chiu, D.T., and Onfelt, B. (2010). Intercellular nanotubes: insights from imaging studies and beyond. Wiley Interdiscip Rev Nanomed Nanobiotechnol *2*, 260–276.

Juhas, M., van der Meer, J.R., Gaillard, M., Harding, R.M., Hood, D.W., and Crook, D.W. (2009). Genomic islands: tools of bacterial horizontal gene transfer and evolution. FEMS Microbiol. Rev. *33*, 376–393.

Kaiser, D. (2008). *Myxococcus*-from single-cell polarity to complex multicellular patterns. Annu. Rev. Genet. *42*, 109–130.

Kearns, D.B., and Shimkets, L.J. (2001). Lipid chemotaxis and signal transduction in *Myxococcus xanthus*. Trends Microbiol. *9*, 126–129.

Koehler, T.M., and Thorne, C.B. (1987). *Bacillus subtilis* (natto) plasmid pLS20 mediates interspecies plasmid transfer. J. Bacteriol. *169*, 5271–5278.

Kolter, R., and Greenberg, E.P. (2006). Microbial sciences: the superficial life of microbes. Nature *441*, 300–302.

Kuchma, S.L., and O'Toole, G.A. (2000). Surface-induced and biofilm-induced changes in gene expression. Curr. Opin. Biotechnol. *11*, 429–433.

Lazazzera, B.A. (2001). The intracellular function of extracellular signaling peptides. Peptides *22*, 1519–1527.

Lederberg, J., and Tatum, E.L. (1946). Gene recombination in Escherichia coli. Nature *158*, 558.

Lemon, K.P., Earl, A.M., Vlamakis, H.C., Aguilar, C., and Kolter, R. (2008). Biofilm development with an emphasis on *Bacillus subtilis*. Curr. Top. Microbiol. Immunol. *322*, 1–16.

Lucas, W.J., Ham, B.K., and Kim, J.Y. (2009). Plasmodesmata - bridging the gap between neighboring plant cells. Trends Cell Biol. *19*, 495–503.

Madigan, M., Martinko, J., and Parker, J., eds. (2003). Brock Biology of Microorganisms, 10th edn (Upper Saddle River, NJ: Pearson Education).

Martens, S., and McMahon, H.T. (2008). Mechanisms of membrane fusion: disparate players and common principles. Nat. Rev. Mol. Cell Biol. *9*, 543–556.

Mashburn-Warren, L.M., and Whiteley, M. (2006). Special delivery: vesicle trafficking in prokaryotes. Mol. Microbiol. *61*, 839–846.

Moons, P., Michiels, C.W., and Aertsen, A. (2009). Bacterial interactions in biofilms. Crit. Rev. Microbiol. *35*, 157–168.

Mulligan, M.E., Murray-Leisure, K.A., Ribner, B.S., Standiford, H.C., John, J.F., Korvick, J.A., Kauffman, C.A., and Yu, V.L. (1993). Methicillin-resistant *Staphylococcus aureus*: a consensus review of the microbiology, pathogenesis, and epidemiology with implications for prevention and management. Am. J. Med. *94*, 313–328.

Mullineaux, C.W., Mariscal, V., Nenninger, A., Khanum, H., Herrero, A., Flores, E., and Adams, D.G. (2008). Mechanism of intercellular molecular exchange in heterocyst-forming cyanobacteria. EMBO J. *27*, 1299–1308.

Nealson, K.H., Platt, T., and Hastings, J.W. (1970). Cellular control of the synthesis and activity of the bacterial luminescent system. J. Bacteriol. *104*, 313–322.

Ng, W.L., and Bassler, B.L. (2009). Bacterial quorum-sensing network architectures. Annu. Rev. Genet. *43*, 197–222.

Nudleman, E., Wall, D., and Kaiser, D. (2005). Cell-to-cell transfer of bacterial outer membrane lipoproteins. Science *309*, 125–127.

Rosenshine, I., Tchelet, R., and Mevarech, M. (1989). The mechanism of DNA transfer in the mating system of an archaebacterium. Science *245*, 1387–1389.

Schara, K., Jansa, V., Sustar, V., Dolinar, D., Pavlic, J.I., Lokar, M., Kralj-Iglic, V., Veranic, P., and Iglic, A. (2009). Mechanisms for the formation of membranous nanostructures in cell-to-cell communication. Cell. Mol. Biol. Lett. *14*, 636–656.

Schleper, C., Holz, I., Janekovic, D., Murphy, J., and Zillig, W. (1995). A multicopy plasmid of the extremely thermophilic archaeon *Sulfolobus* effects its transfer to recipients by mating. J. Bacteriol. *177*, 4417–4426.

Sherer, N.M., Lehmann, M.J., Jimenez-Soto, L.F., Horensavitz, C., Pypaert, M., and Mothes, W. (2007). Retroviruses can establish filopodial bridges for efficient cell-to-cell transmission. Nat. Cell Biol. *9*, 310–315.

Silverman, P.M. (1997). Towards a structural biology of bacterial conjugation. Mol. Microbiol. *23*, 423–429.

Straight, P.D., and Kolter, R. (2009). Interspecies chemical communication in bacterial development. Annu. Rev. Microbiol. *63*, 99–118.

Tanaka, T., and Koshikawa, T. (1977). Isolation and characterization of four types of plasmids from *Bacillus subtilis* (natto). J. Bacteriol. *131*, 699–701.

Tomasz, A. (1965). Control of the competent state in Pneumococcus by a hormone-like cell product: an example for a new type of regulatory mechanism in bacteria. Nature *208*, 155–159.

Tseng, T.T., Tyler, B.M., and Setubal, J.C. (2009). Protein secretion systems in bacterial-host associations, and their description in the Gene Ontology. BMC Microbiol. *9* (*Suppl 1*), S2.

Yang, F., Moss, L.G., and Phillips, G.N., Jr. (1996). The molecular structure of green fluorescent protein. Nat. Biotechnol. *14*, 1246–1251.

EXTENDED EXPERIMENTAL PROCEDURES

Fluorescence Microscopy Procedures

Labeling B. subtilis Cells with Calcein

Exponentially growing *B. subtilis* culture (0.5 ml) was harvested by gentle centrifugation, washed twice with LB medium and resuspended in 0.5 ml fresh LB medium. Next, 10 μl of calcein-AM (1 mg/ml in dimethylsulphoxide, Invitrogen) were added to the medium. The suspension was incubated in the dark at 30°C for 90 min on a rotatory shaker. Subsequently, cells were harvested and washed three times in fresh, dye-free LB medium. Labeled cells were mixed with unlabeled cells in 1:1 ratio, spotted on an agarose pad and visualized by fluorescence microscopy.

Immunofluorescence Microscopy

Immunofluorescence microscopy was carried out as previously described (Ben-Yehuda and Losick, 2002). Blocking solution contained 2% BSA and 10% of an extract from PY79 cells lacking the *cat* gene. Rabbit anti-Cat antibodies (C9336, Sigma) were used at 1:400 dilution, and Rhodamine Red™ donkey anti-rabbit secondary antibodies (711-295-152, Jackson ImmunoResearch) were used at 1:200 dilution.

Fluorescent Images: Processing, Measurement, and Quantification

Quantification of the transfer of calcein and GFP molecules between neighboring cells was carried out as follows: Mixtures of labeled and nonlabeled cells were imaged by time-lapse microscopy and quantification analysis was performed on select fields at the indicated time points. Only nonlabeled cells lying alongside and parallel to labeled cells were considered for this analysis. The distance measurements were estimated by the width of the nonlabeled cells. Cell boundaries were defined by the phase contrast image and the average fluorescence emanating from each cell was determined. The background fluorescence was measured from cell-free regions within a given field and subtracted from the fluorescence values obtained for each individual cell. The fluorescence intensity of a population of cells within a field was determined by averaging the fluorescence intensity from all individual cells residing at the same distance from labeled cells and the standard deviation was calculated accordingly.

EM Procedures

TEM

For whole-cell analysis, cells attached to EM grids were washed with 0.1 M sodium cacodylate buffer (0.1 M, pH 7.2) and fixed with glutaraldehyde (2%) in sodium cacodylate buffer (0.1 M, pH 7.2) for 2 hr at 25°C and cells observed with a Tecnai G^2 Spirit Twin T12 (FEI) operated at 120 kV. TEM images were acquired with a FEI Eagle 4k CCD camera. For cell section analysis, cells attached to the film were washed with 0.1 M sodium cacodylate buffer and fixed with 2.5% GA+ 4% FA in 0.1 M sodium cacodylate buffer (0.1 M, pH 7.2) for O/N at 4°C. Samples were post-fixed in 1% osmium tetroxide for 1 hr at 25°C, dehydrated in a graded series of ethanol and embedded in epoxy resin (Agar 100 Resin Agar Scientific Ltd. Cambridge Essex). The concentration of the resin was increased gradually to 100% in subsequent incubations. Cells attached to the sheets were transferred to prepolymerized epon blocks and subjected for sectioning (70-500 nm). Sections were mounted on thin bar 200 mesh copper grids and stained with uranyl acetate and lead citrate prior to screening. Images were captured on Tecnai 12 electron microscope (FEI, Phillips, Eindhoven, the Netherlands) equipped with MegaView 2 CCD camera and AnalySIS version 3.0 software (Soft Imaging System GmbH, Munster, Germany).

Postembedding Immungold Staining

Immuno-gold analysis was carried out as previously described (Livneh et al., 2009). In brief, *B. subtilis* cells grown on LB agar were gently removed to maintain their spatial organization on solid medium. Removed cells were fixed with 0.25% glutaraldehyde and 2% formaldehyde in 0.1 M PB, pH7.4 for 2 hr at room temperature. Samples were dehydrated in a graded series of ethanol and embedded in 100% LRWhite (London Resin, UK), as previously described (Micheva and Smith, 2007). Ultrathin sections were collected on formvar-coated 200# nickel grids, and processed for postembedding immunogold labeling. Sections were incubated for 30 min in a blocker containing 5% normal goat serum in TBS, followed by 4.5 hr incubation with primary antibody [polyclonal anti-GFP antibodies (Rabbit)]. Next, grids were incubated for 90 min with 12 nm gold-conjugated IgG secondary antibody (1:10 Goat anti Rabbit, Jackson Laboratory), and washed in TBS followed by H_2O (x2). Grids were fixed for 5 min in 2% glutaraldehyde, washed in H_2O (x2) and air-dried. Images were captured on Tecnai 12 electron microscope (FEI, Philips), Eindhoven, the Netherlands) equipped with MegaView 2 CCD camera and AnalySIS version 3.0 software (Soft Imaging System GmbH, Munster, Germany).

Measuring the Frequency of Plasmid Transfer

The following strains were grown separately up to midexponential phase:

P1: SB463: *amyE::*$P_{hyper\text{-}spank}$*-cat-spec* (Cm^R, $Spec^R$)

P1′: GD110: *amyE::*$P_{hyper\text{-}spank}$*-cat-spec*, pHB201/*cat, erm* (Cm^R, $Spec^R$, Mls^R)

P2: GD127: pLS20/*cat* (Cm^R)

P3: SB513: *amyE::*$P_{hyper\text{-}spank}$*-gfp-kan* (Kan^R)

Next, equal number of cells of strains P1, P1′, P2 and P3 were spotted on LB agar separately. In parallel, mixtures of P1+P3, P1′+P3 and P2+P3 were spotted. Spotted cells were grown for 4 hr at 37°C, and then were scratched from the plates and suspended in LB. To determine the frequency of plasmid transfer, cells were diluted and plated in equal numbers onto Cm, Kan and Cm+Kan antibiotic

plates. Plates were incubated O/N at 37°C and CFU/ml were determined. Efficiency of transfer was calculated as ratio between the number of colonies on Cm+Kan divided by the number of colonies on Cm plates (the number of colonies grown on Cm or Kan plates was similar). The results were as follow*:

P1+P3: no colonies obtained on Cm+Kan plates

P1′+P3: 1.0×10^{-7}

P2+P3: 1.2×10^{-4}

*The results are the average of two independent experiments.

DNaseI Resistance Assay

P1′ (GD110: *amyE::P*$_{hyper\text{-}spank}$*-cat-spec*, pHB201/*cat, erm*) (Cm^R, Spec^R, Mls^R), P2 (GD127: pLS20/*cat*) (Cm^R) and P3 (SB513: *amyE::P*$_{hyper\text{-}spank}$*-gfp-kan*) (Kan^R) strains were grown to midexponential phase. Cells of P1′ and P2 were pelleted and washed with 1 x DNaseI buffer (50 mM Tris, pH7.2, 10 mM $MgCl_2$, 5 mM $CaCl_2$), and incubated separately in the presence of 100 μg/ml of DNaseI for 15 min at 37°C in a rotatory shaker. Next, P1′+P3 and P2+P3 were mixed in equal amounts, the mixtures were supplemented with DNaseI (100 μg/ml) and spotted on LB agar. DNaseI buffer (without DNaseI) was added as a control. Spotted cells were grown for 4 hr at 37°C and replica plated on respective antibiotic plates as described in Figure 5. Plasmid transfer was not affected by the presence of DNaseI in both mixtures.

SUPPLEMENTAL REFERENCES

Ben-Yehuda, S., and Losick, R. (2002). Asymmetric cell division in *B. subtilis* involves a spiral-like intermediate of the cytokinetic protein FtsZ. Cell *109*, 257–266.

Branda, S.S., González-Pastor, J.E., Ben-Yehuda, S., Losick, R., and Kolter, R. (2001). Fruiting body formation by *Bacillus subtilis* Proc. Natl. Acad. Sci. USA *98*, 11621–11626.

Chen, L., and Helmann, J.D. (1994). The *Bacillus subtilis* sigma D-dependent operon encoding the flagellar proteins FliD, FliS, and FliT. J. Bacteriol. *176*, 3093–3101.

Cozy, L.M., and Kearns, D.B. (2010). Gene position in a long operon governs motility development in *Bacillus subtilis* Mol. Microbiol. *76*, 273–285.

Guérout-Fleury, A.M., Frandsen, N., and Stragier, P. (1996). Plasmids for ectopic integration in *Bacillus subtilis* Gene *180*, 57–61.

Hashimoto, M., Takahashi, H., Hara, Y., Hara, H., Asai, K., Sadaie, Y., and Matsumoto, K. (2009). Induction of extracytoplasmic function sigma factors in *Bacillus subtilis* cells with membranes of reduced phosphatidylglycerol content. Genes Genet. Syst. *84*, 191–198.

Jerga, A., Lu, Y.J., Schujman, G.E., de Mendoza, D., and Rock, C.O. (2007). Identification of a soluble diacylglycerol kinase required for lipoteichoic acid production in *Bacillus subtilis* J. Biol. Chem. *282*, 21738–21745.

Jones, L.J., Carballido-López, R., and Errington, J. (2001). Control of cell shape in bacteria: helical, actin-like filaments in *Bacillus subtilis* Cell *104*, 913–922.

Jorasch, P., Wolter, F.P., Zähringer, U., and Heinz, E. (1998). A UDP glucosyltransferase from *Bacillus subtilis* successively transfers up to four glucose residues to 1,2-diacylglycerol: expression of *ypfP* in *Escherichia coli* and structural analysis of its reaction products. Mol. Microbiol. *29*, 419–430.

Karmazyn-Campelli, C., Fluss, L., Leighton, T., and Stragier, P. (1992). The spoIIN279(ts) mutation affects the FtsA protein of *Bacillus subtilis* Biochimie *74*, 689–694.

Lemon, K.P., and Grossman, A.D. (1998). Localization of bacterial DNA polymerase: evidence for a factory model of replication. Science *282*, 1516–1519.

Livneh, Y., Feinstein, N., Klein, M., and Mizrahi, A. (2009). Sensory input enhances synaptogenesis of adult-born neurons. J. Neurosci. *29*, 86–97.

López, C.S., Alice, A.F., Heras, H., Rivas, E.A., and Sánchez-Rivas, C. (2006). Role of anionic phospholipids in the adaptation of *Bacillus subtilis* to high salinity. Microbiology *152*, 605–616.

Matsumoto, K., Okada, M., Horikoshi, Y., Matsuzaki, H., Kishi, T., Itaya, M., and Shibuya, I. (1998). Cloning, sequencing, and disruption of the *Bacillus subtilis psd* gene coding for phosphatidylserine decarboxylase. J. Bacteriol. *180*, 100–106.

Meyerovich, M., Mamou, G., and Ben-Yehuda, S. (2010). Visualizing high error levels during gene expression in living bacterial cells. Proc. Natl. Acad. Sci. USA *107*, 11543–11548.

Micheva, K.D., and Smith, S.J. (2007). Array tomography: a new tool for imaging the molecular architecture and ultrastructure of neural circuits. Neuron *55*, 25–36.

Romero, D., Aguilar, C., Losick, R., and Kolter, R. (2010). Amyloid fibers provide structural integrity to *Bacillus subtilis* biofilms. Proc. Natl. Acad. Sci. USA *107*, 2230–2234.

Steinmetz, M., and Richter, R. (1994). Plasmids designed to alter the antibiotic resistance expressed by insertion mutations in *Bacillus subtilis*, through in vivo recombination. Gene *142*, 79–83.

Wach, A. (1996). PCR-synthesis of marker cassettes with long flanking homology regions for gene disruptions in *S. cerevisiae* Yeast *12*, 259–265.

Youngman, P., Perkins, J.B., and Losick, R. (1984). Construction of a cloning site near one end of Tn917 into which foreign DNA may be inserted without affecting transposition in *Bacillus subtilis* or expression of the transposon-borne *erm* gene. Plasmid *12*, 1–9.

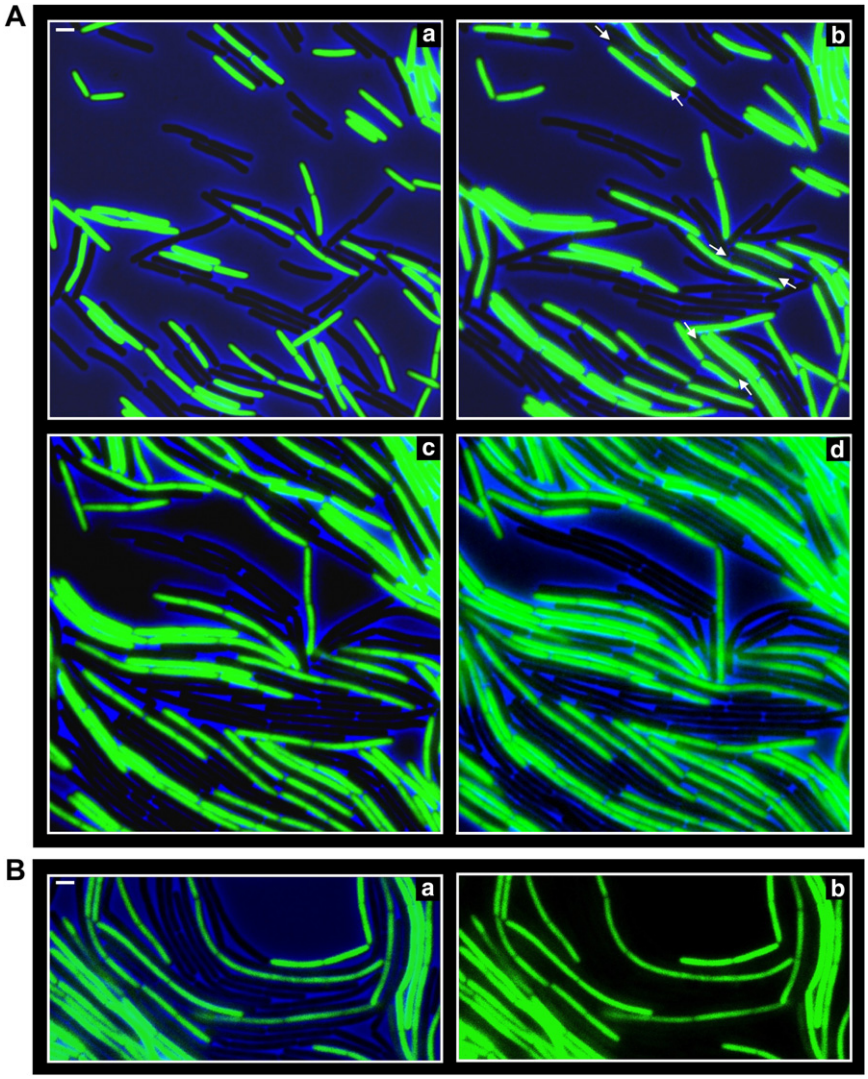

Figure S1. Transfer of GFP Molecules between Neighboring *B. subtilis* Cells, Related to Figure 1

(A) Exponentially growing cells of strains PY79 (*gfp*−) and SB444 (*gfp*+) were mixed, plated on an LB agarose pad, and incubated in a temperature controlled chamber at 37°C. Cells were visualized by time-lapse microscopy and images of phase contrast (blue) and fluorescence (green) were collected at 10 min intervals. Select overlay images are shown from the following time points: (a) t0 min (b) t30 min (c) t60 min and (d) t80 min. Paired arrows in (b) indicate locations where transfer of fluorescent molecules between neighboring cells is initiated. The level of fluorescence emanating from *gfp*− cells increases over time in a manner dependent on distance from *gfp*+ cells. Enlarged images of a selected area are shown in Figure 1C. The scale bar represents 2 μm.

(B) Exponentially growing cells of strains PY79 (*gfp*−) and SB444 (*gfp*+) were mixed, plated on an LB agarose pad, and incubated in a temperature controlled chamber at 37°C. Cells were photographed once, 60 min after the start of incubation. Left: An overlay image of phase contrast (blue) and fluorescence from GFP (green). Right: Fluorescence from GFP. The scale bar represents 2 μm.

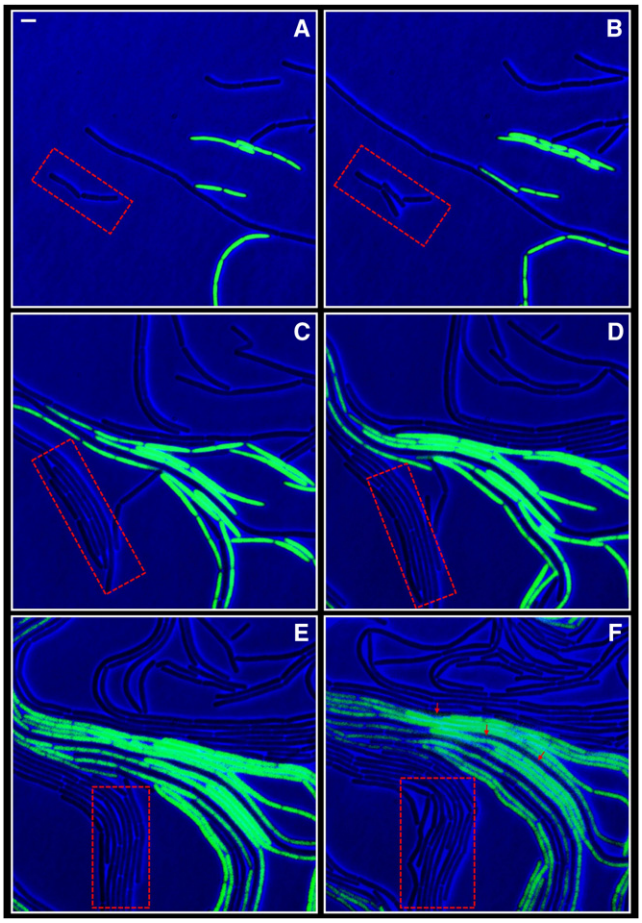

Figure S2. Transfer of GFP Molecules Is Distance Dependent, Related to Figure 1

Exponentially growing PY79 (*gfp*−) and SB444 (*gfp*+) cells were mixed, plated on an LB agarose pad, and incubated in a temperature controlled chamber at 37°C. A region whereby *gfp*+ and *gfp*− cells were distant from each other was selected. Cells were visualized by time-lapse microscopy and images of phase contrast (blue) and fluorescence (green) were collected at 10 min intervals. Select overlay images are shown from the following time points: (A) t0 min (B) t20 min (C) t50 min (D) t70 min (E) t90 min and (F) t110 min. When *gfp*+ and *gfp*− cells are far apart, no fluorescence is detected from *gfp*− cells in all tested time points (dashed rectangular). However, a weak signal is monitored from *gfp*− cells residing in vicinity of *gfp*+ cells at the latest time point (indicated by arrows). The scale bar represents 2 μm.

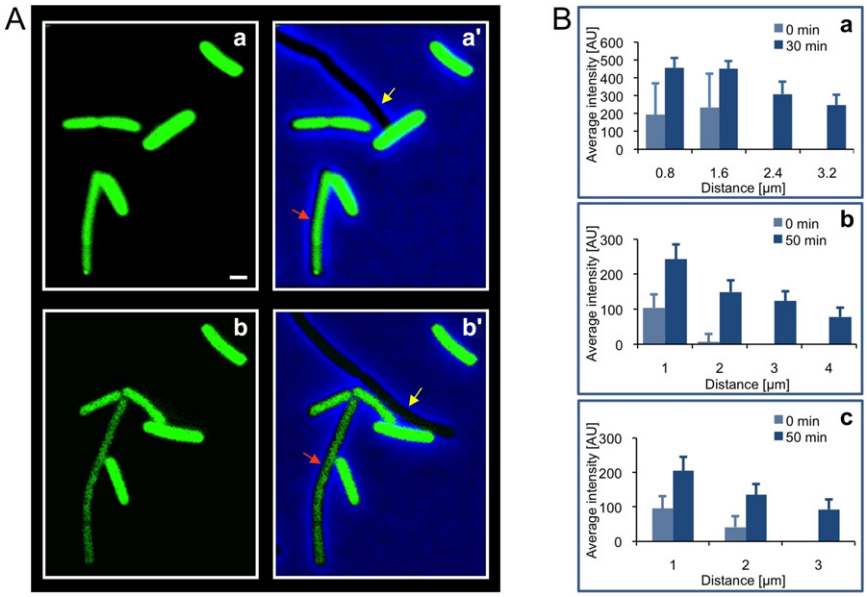

Figure S3. Transfer of Calcein and GFP Molecules between Neighboring Cells Is Distance Dependent, Related to Figures 2, 6, and 7

(A) Exponentially growing PY79 cells were labeled with calcein. Labeled cells were washed and incubated in a temperature controlled chamber at 37°C (see Extended Experimental Procedures). Cells were visualized by time-lapse fluorescence microscopy and images of phase contrast (blue) and fluorescence (green) were collected. Select fluorescence (a and b) and corresponding overlay images (a′ and b′) are shown from the following time points: (a and a′) t0 min (b and b′) t30 min. No significant loss of fluorescence occurred over time. However, when labeled cells underwent cell division (red arrow) or came in contact with a nonlabeled cell in the field (yellow arrow) loss of fluorescence was observed. This decrease in fluorescence is expected since, unlike GFP, calcein is not being regenerated. The scale bar represents 1 μm.

(B) a: Average fluorescence intensity of nonlabeled *B. subtilis* cells as a function of their distance from calcein labeled *B. subtilis* cells at the beginning (0 min; light blue bars) and the end (30 min; dark blue bars) of a coincubation experiment as described in (A). No detectible signal was monitored when cells were located beyond 2 μm at 0 min. Average fluorescence signal is expressed in arbitrary units (AU). Error bars represent standard deviation (SD) of the mean fluorescence signal calculated from at least 40 cells located at the indicated distance. SD for calcein experiments was in general higher than that of the GFP experiments because of variation in labeling efficiency between individual cells. Shown is a representative experiment out of three independent biological repeats. b: Average fluorescence intensity of *S. aureus* (MRSA) (*gfp*−) cells as a function of their distance from *B. subtilis* (*gfp*+) cells at the beginning (0 min; light blue bars) and the end (50 min; dark blue bars) of a coincubation experiment (see Extended Experimental Procedures). No detectible signal was monitored when cells were located beyond 2 μm at 0 min. Average fluorescence signal is expressed in arbitrary units (AU). Error bars represent SD of the mean fluorescence signal calculated from at least 40 cells located at the indicated distance. Shown is a representative experiment out of three independent biological repeats. c: Average fluorescence intensity of *E. coli* (*gfp*−) cells as a function of their distance from *B. subtilis* (*gfp*+) cells at the beginning (0 min; light blue bars) and the end (50 min; dark blue bars) of a coincubation experiment (see Extended Experimental Procedures). No detectible signal was monitored when cells were located beyond 2.5 μm at 0 min. Average fluorescence signal is expressed in arbitrary units (AU). Error bars represent SD of the mean fluorescence signal calculated from at least 40 cells located at the indicated distance. Shown is a representative experiment out of three independent biological repeats.

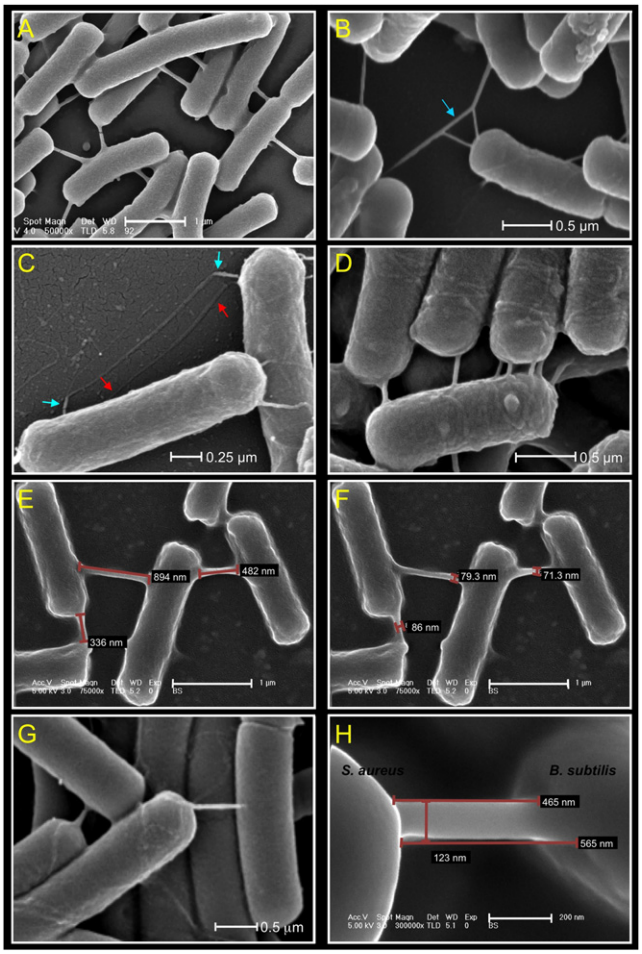

Figure S4. Dimensions and Patterns of Connecting Nanotubes, Related to Figures 3 and 6

B. subtilis and *S. aureus* cells were grown to midexponential phase, plated on LB or minimal medium (S7) agar, incubated for 6 hr at 37°C and visualized by HR-SEM (see Experimental Procedures).

(A) An example demonstrating the multiple nanotubular connections among *B. subtilis* (PY79) cells (×50,000) grown on solid LB medium. The scale bar represents 1 μm.

(B) An example demonstrating junctions of nanotubes (indicated by an arrow) connecting *B. subtilis* (PY79) cells (×30,000) grown on solid LB medium. The scale bar represents 0.5 μm.

(C) An example demonstrating conjugative pili (pairs of colored arrows) connecting two *B. subtilis* cells (GD127) carrying a bona fide conjugative plasmid (pLS20) grown on solid LB medium (×70,000). The scale bar represents 0.25 μm.

(D) An example demonstrating nanotubes formation among *B. subtilis* (3610) cells grown on solid LB medium (×52,000). The scale bar represents 0.5 μm.

(E) Measurement of the length of typical nanotubes connecting *B. subtilis* (PY79) cells (×75,000) grown on solid LB medium. The scale bar represents 1 μm.

(F) Measurement of the width of the nanotubes described in (E). The scale bar represents 1 μm.

(G) An example demonstrating nanotubes formation among *B. subtilis* (PY79) cells grown on solid S7 minimal medium (×24,000). The scale bar represents 0.5 μm.

(H) Measurement of the length and width of a typical nanotube connecting a *B. subtilis* (PY79, right) and a *S. aureus* (MRSA, left) cell (×300,000) grown on solid LB medium. The scale bar represents 200 nm.

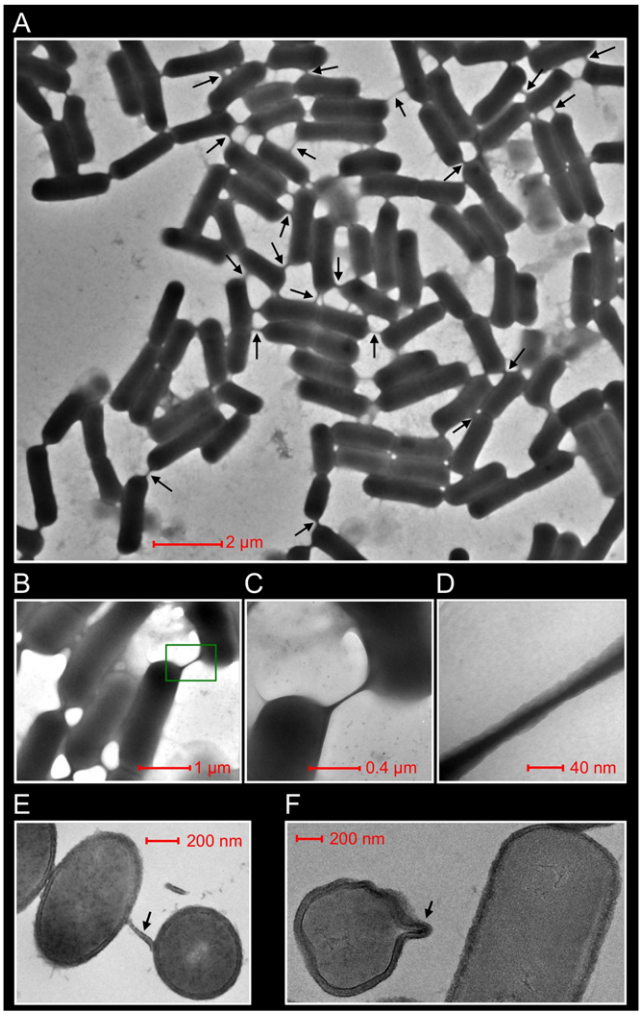

Figure S5. A Network of Nanotubes Connecting *B. subtilis* Cells Observed by TEM, Related to Figure 3

PY79 cells were grown to midexponential phase, plated on LB agar, incubated for 6 hr at 37°C and visualized by TEM (see Extended Experimental Procedures).

(A) A typical field of *B. subtilis* cells demonstrating a network of intercellular nanotubes (×7,500). Arrows indicate examples of nanotubes. The scale bar represents 2 μm.

(B) A view of several *B. subtilis* cells connected by nanotubes (×22,000). The scale bar represents 1 μm.

(C) A higher-magnification image (×100,000) of the region highlighted in (B). The scale bar represents 0.4 μm.

(D) A higher-magnification image (×700,000) of the tube in (C). The scale bar represents 40 nm.

(E) Shown are thin sections (~80 nm) of PY79 cells. Arrow indicates transverse section across a typical nanotube connecting two cells. The scale bar represents 200 nm.

(F) Shown are thin sections (~80 nm) of PY79 cells. Arrow indicates transverse section across a typical protrusion containing cellular content. The scale bar represents 200 nm.

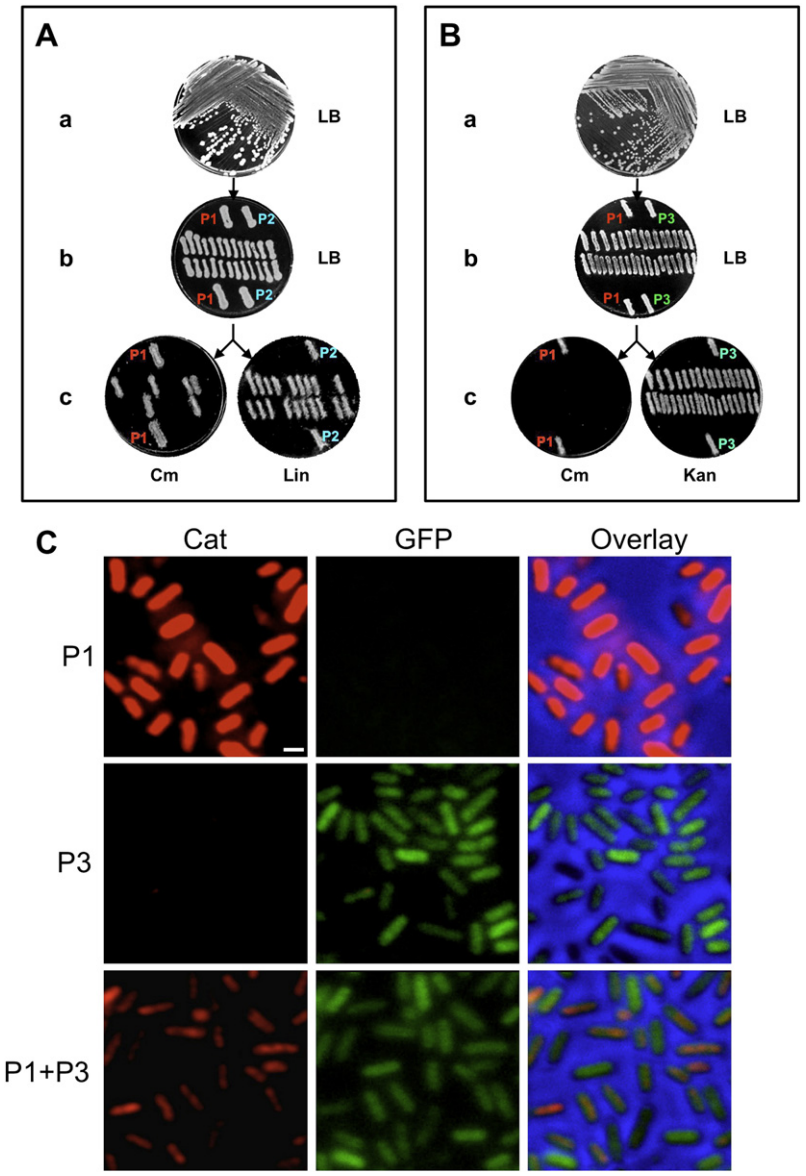

Figure S6. Acquiring Nonhereditary Antibiotic Resistance from Neighboring Cells, Related to Figure 4

(A) An antibiotic assay examining the exchange of Cat and Erm proteins (and possibly transcripts) between two different *B. subtilis* strains (see Figure 4B). a: To analyze the genotype of the colonies growing on the Cm+Lin antibiotic plate shown in Figure 4B, doubly resistant cells were streaked on LB plates and allowed to grow O/N. b: Single colonies were picked, streaked on LB plates and allowed to grow O/N. Parental strains (P1 and P2) were streaked as controls. c: The genotype of the single colonies was tested by replica plating onto Cm and Lin selective plates.

(B) An antibiotic assay examining the exchange of Cat and Kan resistance proteins (and possibly transcripts) between two different *B. subtilis* strains (see Figure 4C). a: To analyze the genotype of the colonies growing on the Cm+Kan antibiotic plate shown in Figure 4C, doubly resistant cells were streaked on LB plates and allowed to grow O/N. b: Single colonies were picked, streaked on LB plates and allowed to grow O/N. Parental strains (P1 and P3) were streaked as controls. c: The genotype of grown streaks was tested by replica plating onto Cm and Kan selective plates.

(C) Equal numbers of cells from P1 (SB463: *amyE::*$P_{hyper\text{-}spank}$*-cat-spec*) (Cm^R) and P3 (SB513: *amyE::*$P_{hyper\text{-}spank}$*-gfp-kan*) (Kan^R, GFP+) were spotted separately on LB agar. In parallel, equal numbers of mixed P1 and P3 cells were spotted similarly. Spotted cells were grown for 6 hr at 37°C. Grown cells were replica plated onto selective plates and finally onto LB as described in Figure 4C. Replica plated P1 cells (grown on Cm plate), P3 cells (grown on Kan plate), and P1+P3 cells (grown on Cm+Kan plate), were scratched from the plates and subjected to immunofluorescence microscopy with anti-Cat antibodies (see Extended Experimental Procedures). Left: Signal from anti-Cat antibodies (red), Middle: Signal from GFP (green), Right: Overlay of red and green signals with a phase contrast image (blue). Fluorescence images have been normalized to a similar intensity range. The scale bar represents 1 μm.

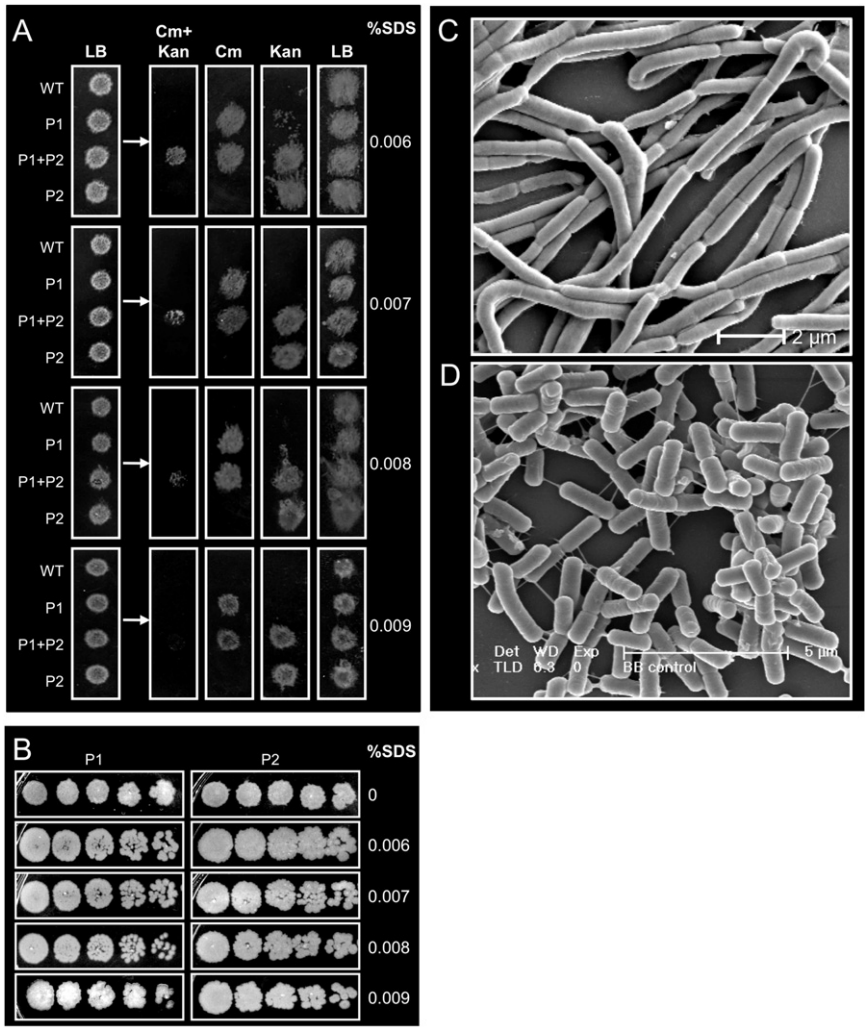

Figure S7. Inhibition of Nanotube Formation by SDS, Related to Figure 4

(A) An antibiotic assay examining the transfer of Cat protein under different SDS concentrations. Left: equal numbers of cells from PY79 (WT), SB463 (*amyE::*$P_{hyper\text{-}spank}$*-cat-spec*) (P1: Cm^R) and SB513 (*amyE::*$P_{hyper\text{-}spank}$*-gfp-kan*) (P2: Kan^R) strains were spotted separately on LB agar plates containing the indicated amounts of SDS. In parallel, equal numbers of mixed P1 and P2 cells (1:1) were spotted similarly. Spotted cells were grown for 4 hr at 37°C. Right: grown cells were replica plated onto the indicated plates supplemented with SDS. Plates were incubated O/N at 37°C.

(B) P1 and P2 strains were grown to midexponential phase and spotted in serial dilutions (3^{-6}-3^{-10}) on LB agar containing SDS at the indicated concentrations. To rule out the possibility that SDS increases antibiotic sensitivity, plates were supplemented with Cm for P1 and Kan for P2. Cells were photographed after O/N. In general, cells spotted on SDS containing plates spread more in diameter than cells spotted on plates without SDS. On high SDS concentrations cell growth was delayed; however, as evidence here, the viability was not significantly reduced.

(C) Wild-type PY79 cells were grown to midexponential phase, plated on LB agar containing 0.007% SDS, incubated for 6 hr at 37°C and visualized by HR-SEM (see Experimental Procedures). Shown is a typical field of cells evidently lacking visible nanotubes (×10,000). The scale bar represents 2 μm. In general, cells grown in the presence of SDS appeared in long chains and frequently failed to stick to the EM grids properly. This made it difficult to visualize cells growing at higher SDS concentrations.

(D) PY79 cells were grown to midexponential phase as in (C) in the absence of SDS and visualized by HR-SEM. Shown is a typical field of cells whereby a network of intercellular connecting nanotubes is evident (×10,000). The scale bar represents 5 μm.